Published in final edited form as:
J Immunol. 2015 February 15; 194(4): 1983–1995. doi:10.4049/jimmunol.1402481.

TLR signaling modulates side effects of anticancer therapy in the small intestine

Magdalena Frank[*,‡], **Eva Maria Hennenberg**[*,‡], **Annette Eyking**[*,‡], **Michael Rünzi**[†,‡], **Guido Gerken**[*,‡], **Paul Scott**[§], **Julian Parkhill**[§], **Alan W. Walker**[§,¶], and **Elke Cario**[*,‡]

[*]Div. of Gastroenterology and Hepatology, University Hospital of Essen, Germany

[†]Div. of Gastroenterology and Metabolic Diseases, Kliniken Essen Süd, Essen, Germany

[‡]Medical School, University of Duisburg-Essen, Essen, Germany

[§]Pathogen Genomics Group, Wellcome Trust Sanger Institute, Wellcome Trust Genome Campus, Hinxton, Cambridge, UK

[¶]Microbiology Group, Rowett Institute of Nutrition and Health, University of Aberdeen, Aberdeen, UK

Abstract

Intestinal mucositis represents the most common complication of intensive chemotherapy, which has a severe adverse impact on quality of life of cancer patients. However, the precise pathophysiology remains to be clarified and there is so far no successful therapeutic intervention. Here, we investigated the role of innate immunity through TLR signaling in modulating genotoxic chemotherapy-induced small intestinal injury *in vitro* and *in vivo*. Genetic deletion of TLR2, but not MD-2, in mice resulted in severe chemotherapy-induced intestinal mucositis in the proximal jejunum with villous atrophy, accumulation of damaged DNA, $CD11b^+$-myeloid cell infiltration and significant gene alterations in xenobiotic metabolism, including a decrease in ABCB1/MDR1 p-glycoprotein (p-gp) expression. Functionally, stimulation of TLR2 induced synthesis and drug efflux activity of ABCB1/MDR1 p-gp in murine and human $CD11b^+$-myeloid cells, thus inhibiting chemotherapy-mediated cytotoxicity. Conversely, TLR2 activation failed to protect small intestinal tissues genetically deficient in MDR1A against DNA-damaging drug-induced apoptosis. Gut microbiota depletion by antibiotics led to increased susceptibility to chemotherapy-induced mucosal injury in wildtype mice, which was suppressed by administration of a TLR2 ligand, preserving ABCB1/MDR1 p-gp expression. Findings were confirmed in a preclinical model of human chemotherapy-induced intestinal mucositis using duodenal biopsies, by demonstrating that TLR2 activation limited the toxic-inflammatory reaction and maintained assembly of the drug transporter p-gp. In conclusion, this study identifies a novel molecular link between innate immunity and xenobiotic metabolism. TLR2 acts as a central regulator of

Corresponding author: Prof. Dr. med. Elke Cario; Experimental Gastroenterology, Div. of Gastroenterology and Hepatology, University Hospital of Essen, Institutsgruppe I, Virchowstr. 171; D-45147 Essen, Germany. Phone: +49 201 723 4527; fax: +49 201 723 6858; elke.cario@uni-due.de.

Disclosures
The authors have no financial conflicts of interest.

Europe PMC Funders Author Manuscripts

xenobiotic defense via the multidrug transporter ABCB1/MDR1 p-gp. Targeting TLR2 may represent a novel therapeutic approach in chemotherapy-induced intestinal mucositis.

Introduction

Intestinal mucositis represents a major oncological problem (1). It is the most common complication of intensive chemotherapy, which has a severe adverse impact on quality of life, morbidity and mortality of cancer patients. Importantly, mucositis may require delays in scheduled chemotherapy cycles, thereby potentially reducing the efficacy of anti-cancer treatment and thus the chance of remission. Intestinal mucositis occurs in up to 100% of patients undergoing high-dose chemotherapy with stem cell or bone marrow transplantation for hematological or solid tumors (1). Gastrointestinal toxicity is the major dose-limiting factor for anti-cancer drugs, such as methotrexate (MTX), an effective chemotherapeutic agent often used to treat many cancers in pediatric and adult patients (2). The condition may affect the entire gastrointestinal tract and causes severe pain, diarrhea and weight loss. However, despite the severity and prevalence of chemotherapy-induced intestinal mucositis, there is so far no successful therapeutic intervention that prevents or treats all symptoms of disease (3).

The precise pathophysiology underlying chemotherapy-induced intestinal mucositis has not been clarified yet. Current understanding suggests the culmination of a dynamic sequence of complex inflammatory events that are initiated by direct chemotherapy-induced injury to crypt cells and cells in the underlying mucosal tissue (4). In addition, chemotherapy-induced diarrhea has been associated with potential alterations in microbiota composition (5, 6), which may contribute to dysregulated mucosal immune responses. The gut microbiota may modulate intestinal metabolism of xenobiotics and anticancer drugs (7), thus potentially inducing or inhibiting gut toxicity. For instance, ß-glucuronidase produced by *E. coli* generates SN-38, a toxic metabolite of irinotecan, which directly damages the intestinal mucosa (8). The indigenous microbiota may also influence endogenous xenobiotic detoxification (9), however, the innate immune mechanisms of host-chemotherapy drug interactions and their role in triggering adverse effects have not yet been delineated.

Commensal bacterial ligands are recognized by Toll-like receptors (TLRs) (10). Recent findings, mainly derived from murine colitis models, imply that this constant interaction ensures mucosal homeostasis through restrained inflammatory responses and accelerated restitution and healing in the healthy colon (11). Mice deficient in TLR2/4/5 or MyD88 exhibit delayed or diminished tissue repair responses during acute DSS (Dextran Sulfate Sodium)-induced colonic inflammation (12-16). The gut microbiota may differentially modulate mucosal TLR responsiveness in a susceptible host, thus subverting immune responses to a predominantly pro-inflammatory phenotype (11). It has been postulated that aberrant microbiota-TLR signaling may be involved in the pathogenesis of chemotherapy-induced mucositis (17, 18), but direct experimental evidence is so far lacking.

Transmembrane p-glycoprotein (p-gp) functions as an ATP-dependent efflux transporter pump to prevent cellular accumulation of numerous xenobiotics and drugs, including antineoplastics (19, 20). Induction of p-gp results from ABCB1/MDR1 transcriptional and

Europe PMC Funders Author Manuscripts

translational activation. P-gp is expressed by many different cell types, including monocytes/macrophages and intestinal epithelial cells (21). As a central member of the superfamily of ABC transporters, p-gp interacts with many drug-metabolizing enzymes in a complex network and absence of p-gp can lead to severe drug toxicity (22). ABCB1/MDR1 polymorphisms (23) may alter drug levels and host susceptibility to diseases, such as inflammatory bowel diseases. Mice deficient in MDR1A show increased susceptibility to microbiota-induced colitis (24, 25) and radiation-mediated intestinal injury (26). Genetic disruption of MDR1A may contribute to intestinal dysbiosis (27). Furthermore, p-gp expression may be differentially modulated by various mediators, including intestinal bacteria (28, 29), yet the signaling mechanisms remain to be determined.

In this study, we identify a novel molecular link between innate immunity and xenobiotic metabolism and show its implication in host detoxification and protection against chemotherapy-induced side effects in the small intestine. We demonstrate that TLR2-mediated activation of ABCB1/MDR1-encoded p-gp in $CD11b^+$-myeloid cells critically controls the severity of methotrexate-associated gut toxicity. Our findings provide a rationale for developing new drugs for the management of cancer therapy-induced mucosal damage in the gastrointestinal tract based on commensal-mediated innate immune modulation via TLR2.

Materials and Methods

Reagents and antibodies

The synthetic lipopeptide Pam_3Cys-SKKKK×3HCl ($Pam_3CysSK4$ (PCSK); lot A15) was obtained from EMC Microcollections and dissolved in sterile water (vehicle control). Methotrexate (MTX) was obtained from Pfizer and sterile saline was used as vehicle control; Fluorescein (FL)-MTX was from Life Technologies, respectively. The specific p-gp inhibitor (C-4), a cell-permeable cinnamoyl compound that reversibly inhibits p-gp efflux function (30), was from Merck and dissolved in DMSO (vehicle control). CD11b and CD4 antibodies were from BD Pharmingen. P-glycoprotein (C219) antibody was from Merck, DUSP-1 from Santa Cruz Biotechnology and phospho-MKK3/6, phospho-p38 MAPK, p38 MAPK, phospho-histone H3, phospho-histone H2A.X, phospho-ß-catenin and cleaved PARP antibodies were from Cell Signaling. Rabbit polyclonal anti-TFF3 (HM5119) antibody was kindly provided by Dr. D. K. Podolsky. Alexa Fluor® 488- or 350-conjugated goat anti-rabbit, anti-mouse or anti-rat IgG antibodies were from Life Technologies and HRP-conjugated anti-rabbit and anti-mouse antibodies were from GE Healthcare. All other reagents were obtained from Sigma-Aldrich, unless otherwise specified.

Animals

TLR2 knockout (KO; B6.129-*Tlr2*^{tm1Kir}/J; Jackson Laboratory) (31) and MD-2 KO (32) (kindly provided by Dr. Kensuke Miyake, University of Tokyo, Japan) mice [all C57BL6/J; >F10] were intercrossed for double knockout (dKO) homozygotes (TLR2/MD-2 dKO); wildtype (WT) C57BL6/J mice were used as controls. WT and MDR1A KO (FVB.129P2-*Abcb1a*^{tm1Bor} N7; originally developed by Dr. Alfred Schinkel, The Netherlands Cancer Institute) (20) mice [all FVB/N; >F7] were obtained under crossbreeding agreement from

Taconic Farms (Germantown, NY). All mice were bred and housed in the same temperature- and humidity-controlled room on a 12-hour light-dark cycle under strict specific-pathogen-free conditions (Central Animal Facility, University Hospital of Essen, Germany). All animals were provided *ad libitum* with autoclaved tap water and autoclaved pelleted laboratory chow (ssniff® M-Z, ssniff Spezialdiäten GmbH, Soest, Germany) containing folic acid (10 mg/kg). Extensive animal health monitoring (FELASA criteria) was conducted routinely on sentinels from this room and no pathogens were detected. Mice were confirmed to be the desired genotype via standard genotyping techniques. For studies, only age-matched female mice were used, as indicated. For microbiota analysis, successive litters of individual heterozygous breeding pairs were analyzed to control for maternal influence; offspring were housed on the same rack but individually in cages to avoid synchronization, as previously described (33). Protocols were in compliance with German law for use of live animals and reviewed and approved by the local animal protection officer at the University Hospital of Essen and the responsible district government.

Murine and human cells

Primary murine myeloid cells flushed from femurs were isolated from female mice aged ~5 weeks, passed through a 100 μm-cell strainer (BD Falcon) and purified using the EasySep CD11b Positive Selection Kit (Stemcell). Murine bone-marrow derived $CD11b^+$-myeloid cells were cultured on Poly-D-Lysine-coated (BD BioCoat) tissue culture plastic in Leibovitz's L-15 medium (Life) supplemented with 10% v/v FBS (Thermo or PAA) and penicillin/streptomycin (Life) in an air incubator at 37°C. Human $CD11b^+$-myeloid (34) monocytic-like THP-1 cells (TIB-202; passages #13-#19) were obtained from the American Type Culture Collection (ATCC) and maintained in RPMI1640 medium (PAA or Life) supplemented with 10% v/v FBS, 2 mM L-glutamine (Life) and penicillin/streptomycin in a humidified incubator at 37°C with 5% CO_2. The intestinal epithelial cell line Caco-2 (HTB-37; #11-#15) was purchased from ATCC and maintained as described previously (35).

Murine model of chemotherapy-induced intestinal mucositis

A common murine model of chemotherapy-induced mucositis was applied by *i.p.* injection of MTX [40 mg/kg BW/d; for 4 days] in female mice aged ~9 weeks. For microbiota depletion, mice were treated with antibiotics (vancomycin (ratiopharm) and imipenem (MSD) [both 50 mg/kg BW/d] in drinking water (36)) for 5 days prior to MTX treatment [40 mg/kg BW/d; for 2 days]. Short intake of vancomycin and imipenem has been shown to notably reduce gut microbial load and diversity (37). Six hours after finishing antibiotic treatment, PCSK (150 μg/ml) was added to fresh drinking water starting one day prior to MTX, renewed every other day and stopped on day 5. Mice were sacrificed on day 7, or as indicated otherwise. Mortality rate includes mice that had to be sacrificed due to severe morbidity, including loss of >20% body weight. For histologic evaluation, frozen cross-sections (7 μm) of murine proximal jejunum, terminal ileum or distal colon were stained with H&E (Fast Frozen Stain Kit; Polysciences). Histologic severity of mucositis was assessed by blinded scoring (Suppl. Table I). Aperio ScanScope® system (Aperio Technologies, USA) was used to capture and visualize high resolution images of tissue sections (ImageScope version 11.2.0.780).

Organ culture of mucosal biopsies of human small intestine

Small duodenal specimens from a total of 7 Caucasian patients (median age: 64 years) undergoing screening esophagogastroduodenoscopy for gastroesophageal reflux disease were freshly obtained at the Endoscopy Unit, Department of Gastroenterology and Metabolic Diseases, Kliniken Essen Süd, an affiliate of the University Hospital of Essen. Informed consent was obtained from all patients before the procedure, and the protocol was approved by the Human Studies Committee of the Medical Faculty, University of Duisburg-Essen. All patients underwent preprocedural fasting for at least 8 hours (no medication). Macroscopically and microscopically, the morphology of the duodenal mucosa was normal in all cases. The samples were immediately washed in ice-cold Hanks' buffered salt solution (PAA or Life) supplemented with 10% v/v FBS, gentamicin (Life), and antibiotic/antimycotic solution (PAA); then mixed into a thin layer of cold liquid Matrigel (BD Biosciences) with or without PCSK (20 μg/ml), which was allowed to form a gel at 37°C within 30 min; then covered with warm full L-15 medium with or without MTX (10 μM); and cultured for 3.5 h. Matrigel biopsy blocks were snap frozen in liquid nitrogen, embedded in Tissue-Tek OCT compound (Sakura), and stored at −80°C until further processing.

Flow cytometry analysis of p-gp function

The fluorochromes rhodamine 123 and $DiOC_2(3)$ represent substrates for transport mediated by p-gp (38). The functional efflux activity of p-gp was assessed using the Multidrug Resistance Direct Dye Efflux Assay kit (Millipore), according to the manufacturer's instructions with minor modifications. In brief, after stimulation with or without PCSK (20 μg/ml), THP-1 cells were loaded with rhodamine 123 for 1 h or $DiOC_2(3)$ for 15 min on ice and washed and dye efflux was initiated by incubating the cells for 1 h at 37°C. To assess efflux of MTX, THP-1 cells were incubated with FL-MTX (10 μM) for 21 h, washed and stimulated with or without PCSK (20 μg/ml) for 3 h or THP-1 cells were pretreated with the p-gp inhibitor (10 μM) or vehicle (DMSO) for 15 min, stimulated with or without PCSK (20 μg/ml) for 5 min, washed and incubated with FL-MTX (10 μM) for 21 h. After washing, cells (3×10^4/sample) were analysed using a FACSCanto™ II (BD Biosciences). Dead cells were excluded by forward/side scatter and flow cytometry data were analyzed using FlowJo software for PC (version 7.6.5; Tree Star).

Immunofluorescence

Frozen sections of tissues were cut (7 or 10 μm) and mounted on Superfrost Plus Gold slides (Thermo). Dependent on primary antibodies, sections were fixed with either acetone (100%) for 5-10 min at −20°C or paraformaldehyde (3-4%) for 15 min at RT. Sections were blocked with normal goat serum (1:10-1:20 in PBS, ± 0.3% TX-100 (Thermo)) for 60 min at RT and incubated with primary antibodies (1:50-1:1000; for anti-p-gp: 5 μg/ml) o/n at 4°C. Fluorescent-labeled antibodies were used as secondary antibodies (1:50-1:100, 60 min, RT). After mounting with Vectashield Mounting Medium with DAPI or PI (Vector Laboratories) or TO-PRO-3 (Life), immunofluorescent sections were assessed by using optical sectioning with confocal (Axiovert 100M with laser scan head LSM 510) or structured illumination (AxioObserver.Z1 with ApoTome) microscopes (Zeiss, Germany). The multitrack option

and sequential scanning for each channel were used to eliminate any cross talk of the chromophores and to ensure reliable co-localization results with the combination of Alexa Fluor® dyes 350 and 488. Control experiments were performed with isotype control IgG (Santa Cruz).

Analysis of apoptosis in murine small intestinal tissues

Murine small intestinal tissues from female mice aged ~9 weeks were cultured short-term *ex vivo*, as previously described (14), except that samples were stimulated with or without PCSK (20 μg/ml) for 30 min and then exposed to MTX (10 μM) for 4 h. Matrigel-attached small intestinal tissues were immediately processed for analysis of apoptosis (in situ cell death detection kit, fluorescein; Roche) by quantifying TUNEL-positive cells in relation to the total number of PI-labeled nuclei (>1,000 cells per condition) using ImageJ (NIH) in a random collection of captured 40x images by epifluorescence microscopy.

Myeloperoxidase assay

Myeloperoxidase (MPO) activity was determined by commercially available MPO assay (Mouse MPO ELISA kit; Hycult Biotech), according to the manufacturer's instructions. Briefly, proximal jejunal tissue harvested from mice was lysed (5 mg/100 μl) in ice-cold lysis buffer (10% glycerin, 200 mM NaCl, 10 mM Tris-HCl (pH 7.4), 5 mM EDTA, supplemented with PhosSTOP Phosphatase and complete Mini protease inhibitor cocktail tablets (Roche), and 1 mM PMSF), followed by grinding in a bead mixer mill (MM301, Retsch, Haan, Germany). Protein content in the supernatant was determined by Bradford protein assay (BioRad).

Protein analysis by immunoblotting

For preparation of whole cell lysates, cells were rinsed once in cold PBS (without Ca^{2+}/Mg^{2+}) with 100 μM Na_3VO_4 and then lysed in ice-cold lysis buffer (1% TX-100, 150 mM NaCl, 20 mM Tris-HCl (pH 7.5), 2 mM EDTA, supplemented with PhosSTOP Phosphatase and complete Mini protease inhibitor cocktail tablets, and 1 mM PMSF). Immunoblotting was performed as previously described (39). To confirm equal protein loading, blots were reprobed with anti-ß-actin. Representative blots of at least two independent experiments are shown.

RNA/DNA extraction

Total RNA from cells or tissues was extracted (RiboPure; Ambion) and purified including the RNase-free DNase digestion step (RNeasy Mini Kit; Qiagen). Genomic DNA from full thickness proximal jejunum samples containing liquid stool was isolated (FastDNA™ SPIN Kit for Soil; MP Biomedicals) and processed by the BIO101/Savant FastPrep® FP120 homogenizer, according to the manufacturer's instructions.

Microarray analysis

All RNA samples from murine proximal jejuna (n = 3 per condition) were analyzed independently and further processed at MFT Services (Tübingen, Germany) using GeneChip® Mouse Gene 1.1 ST arrays (Affymetrix). Hybridization, washing, staining and

scanning was performed automatically in a GeneTitan® instrument (Affymetrix). Data were normalized with RMA (Robust Multichip Average) to yield log2-transformed signal values which were then averaged for the individual subgroups. Probe sets with low variance over all samples were regarded as non-informative and removed from the data set. Data have been deposited in GEO (GSE56426). Data were further analyzed, as previously described (40), through 1) hierarchical clustering analysis and plotting as a heat map using the ArrayStar software (DNAStar) and 2) Ingenuity Pathways Analysis (Ingenuity Systems®, www.ingenuity.com).

Real-time PCR for gene expression analysis

QuantiTect Primer Assays (Qiagen) were used as the gene-specific murine or human primer pairs. Quantitative real-time RT-PCR was performed using the one-step QuantiFast SYBR Green RT-PCR kit (Qiagen) on the Mastercycler ep realplex (Eppendorf) real-time amplification system. Copy numbers of individual transcripts were related to Gapdh as endogenous control (×/100,000 copies Gapdh) and normalized as indicated.

Analysis of microbiota composition

DNA extracted from murine proximal jejunum samples was used as a template for PCR amplification using barcoded fusion primers MiSeq-27F (5′-AATGATACGGCGACCACCGAGATCTACACTATGGTAATTCCAGMGTTYGATYM T GGCTCAG-3′) and MiSeq-338R (5′-CAAGCAGAAGACGGCATACGAGAT-barcode-AGTCAGTCAGAAGCTGCCTCCCGTAGGAGT-3′), which target the V1-V2 regions of the bacterial 16S rRNA gene and contain adaptors for downstream Illumina MiSeq sequencing. A unique barcoded reverse primer was used for each of the individual proximal jejunum samples. PCR was carried out using Q5™ Taq polymerase (New England Biolabs) and cycling conditions were: 98°C for 2 min, then 20 cycles of 98°C for 30 sec, 50°C for 30 sec, 72°C for 90 sec and then a final 72°C extension step for 5 min. Four reactions were carried out per sample. Pooled amplicons were then ethanol precipitated in order to concentrate to 25 μl volumes per sample which were then quantified using a Qubit 2.0 Fluorometer (Life) and equimolar concentrations of each sample were added together to a sequencing mastermix. Sequencing was done at the Wellcome Trust Sanger Institute on an Illumina MiSeq machine using 2 × 250 bp read length. Sequence data from all mice (#1-#16) have been deposited in the European Nucleotide Archive (http://www.ebi.ac.uk/ena; accession numbers: #1: ERS563915; #2: ERS563916; #3: ERS563898; #4: ERS563909; #5: ERS563897; #6: ERS563899; #7: ERS563900; #8: ERS563901; #9: ERS563903; #10: ERS563904; #11: ERS563906; #12: ERS563907; #13: ERS563902; #14: ERS563905; #15: ERS563908; #16: ERS563910). The Illumina sequence data was processed using the mothur software package (41), closely following their MiSeq SOP (42). To summarize the steps involved: forward and reverse read MiSeq data were assembled into paired-read contigs and then all resulting contigs that were shorter than 260 bp, longer than 450 bp, contained any ambiguous bases, or contained homopolymeric stretches longer than 7 bases were removed. Putative chimeric sequences were removed using Perseus software (43) incorporated into mothur. Also removed were any reads that were derived from chloroplasts, mitochondria, eukarya, or archaea. Following these quality control steps 102,373 sequences remained in the final dataset (range of 31 to 19,716 sequences per sample). Three mice (#4, #12, #14)

Europe PMC Funders Author Manuscripts

had to be excluded from final analysis, as there were not enough sequence data to give reliable results. Samples from 13 mice remained (range of 1223 to 19,716 sequences per sample).

A pre-clustering step (*diffs* = 3) was carried out to reduce the impact of sequencing errors and then operational taxonomic units (OTUs) were generated at a 97% similarity cut-off level. Each OTU was given a taxonomic classification using the RDP (Ribosomal Database Project) reference taxonomy provided for use with the mothur software package. Metastats (44), utilized in mothur, was used to test for significant differences in the proportional abundance of individual OTUs, as well as taxonomic groupings at the Phylum, Family and Genus levels. As multiple independent comparisons were carried out, significance was set at $p < 0.01$. To measure bacterial diversity the dataset was first randomly sub-sampled to 1084 sequences per sample to ensure equal sequencing depth among each of the samples. Following this step, observed diversity (i.e. the number of observed OTUs) and Shannon diversity indices for each sub-sample were calculated in mothur. To test whether there were any significant difference in diversity between the mouse cohorts Kruskall-Wallis and Mann Whitney U tests were carried out using Minitab (v16). To assess whether or not there were significant microbiota clustering patterns associated with chemotherapy, the sub-sampled dataset was then used to create a cluster dendrogram, using the Bray Curtis calculator, in mothur. The resulting dendrogram was visualised using the iTOL online software tool (45).

Statistical analysis

The unpaired, two-tailed t-test was used to calculate differences between means (GraphPad Prism version 5.04, GraphPad Software), if not indicated otherwise. Survival data were analyzed using the log-rank test. A p value of <0.05 was considered as significant. All data are expressed as the means ± SEM.

Results

Loss of TLR2 results in severe chemotherapy-induced intestinal mucositis in mice

To investigate the functional role of central innate immune regulators in modulating side effects of anti-cancer therapy in the small intestine, mice lacking TLR2 or MD-2 (an essential co-receptor of TLR4 signaling) were exposed to a common model of chemotherapy-induced intestinal mucositis by systemically administering high-dose methotrexate (MTX), as described in *Materials and Methods*. In contrast to MTX-WT or MTX-MD-2 KO, all MTX-TLR2 KO mice were highly susceptible to chemotherapy-induced small intestinal injury (Fig. 1). Microscopic inflammation in the small intestine from MTX-TLR2 KO mice on day 7 was characterized by villous atrophy, crypt ablation, intestinal epithelial damage and evidence of inflammatory cell infiltrates in the lamina propria, which were not present in MTX-WT or MTX-MD-2 KO animals (Fig. 1A). Severe inflammation was histologically evident in all areas of the small intestine of MTX-TLR2 KO mice, with a mean mucositis score of 12.8±0.2 in the proximal jejunum and 8.0±0.4 in the terminal ileum (Fig. 1B), which was paralleled clinically by significant weight loss (Fig. 1C). This was significantly greater than the mean mucositis scores for WT (proximal jejunum: 1.6±0.4; terminal ileum: 2.6±0.9) or MD-2 KO (1.8±0.4; 1.2±0.5) mice after MTX

treatment, which showed relatively normal intestinal architectures comparable to healthy controls and no weight loss. Furthermore, small intestinal myeloperoxidase (MPO) activity, an indicator of oxidative damage, was markedly enhanced after MTX treatment only in the absence of TLR2 (Fig. 1D). Of note, TLR2 KO mice developed consistently severe mucositis in response to MTX, regardless of litters, cages and time of experiment. These results suggest that functional TLR2 signaling in the small intestinal mucosa may be critical for protection against chemotherapy-induced side effects.

Deletion of MD-2 in TLR2 KO mice completely abolished the destructive gut mucosal inflammation in response to chemotherapy (Fig. 1A-D). TLR2/MD-2 dKO mice appeared healthy (no significant weight loss) and mean histology scores (proximal jejunum: 1.7±0.2; terminal ileum: 1.7±0.3) resembled those of MTX-WT or MTX-MD-2 KO controls. These findings imply that LPS signaling via MD-2/TLR4 may be responsible for the exacerbation of chemotherapy-induced small intestinal mucositis in the context of TLR2 deficiency.

Chemotherapy induces genotoxicity and alterations in xenobiotic metabolism in the small intestine of TLR2 KO mice

We further characterized the extensive mucosal barrier injury seen in severe chemotherapy-induced mucositis in TLR2 deficiency. Immunofluorescent staining of MTX-TLR2 KO proximal jejuna demonstrated aberrant accumulation of $CD11b^+$-myeloid cells, but not $CD4^+$ T cells, in the inflamed lamina propria (Fig. 2A). These early cell infiltrates showed fulminant genotoxic stress in response to MTX (Fig. 2B), as evidenced by the presence of double-strand DNA breaks (phosphorylated histone H2A.X) and abnormal mitoses (phosphorylated histone H3). Disruption of intestinal epithelial barrier integrity was emphasized by dramatic depolarization of phosphorylated ß-catenin and goblet cell depletion during MTX-induced genotoxic stress (Fig. 2C).

Next, we analyzed the impact of chemotherapy on the overall microbial composition and structure in the proximal jejunum by Illumina MiSeq-based analysis of bacterial 16S rRNA genes. There were no statistically significant differences in bacterial diversity between MTX-TLR2 KO and MTX-WT proximal jejunum samples on day 7, or when compared to healthy controls, respectively (Suppl. Fig. 1A, B). Compositional analysis of the microbiota indicated that there was a high degree of variation between mice. One TLR2 KO mouse (#13) showed overgrowth with *Enterobacteriaceae* in response to MTX. Nevertheless, individual samples of the same group did not show any distinct clustering patterns and no broad-scale compositional differences and signatures were identified between groups (Fig. 3). These data suggest that MTX-induced intestinal mucositis in combination with or without genetic deletion of TLR2 may not provoke consistent shifts in microbiota community structure in the proximal jejunum.

To gain further insight into the underlying host mechanisms responsible for the severity of chemotherapy-induced genotoxic injury in the context of TLR2 deficiency, we performed a broad gene expression profiling analysis to identify potential target genes. We compared mRNA expression levels in proximal jejunal tissues between healthy and MTX-exposed WT vs. TLR2 KO mice. Through hierarchical clustering of the microarray data sets (Fig. 4A, Suppl. Table II), we identified 409 genes significantly regulated with >8-fold differential

expression (MTX-TLR2 KO vs. WT control). Within this set, 140 genes were most differentially regulated between MTX-TLR2 KO and MTX-WT (log2 ratio cutoff, 4.0) and belonged predominantly to canonical pathways associated with xenobiotic metabolism (Fig. 4B, Suppl. Table IIIA, B), as annotated by the Ingenuity knowledge base. Real-time RT-PCR analysis of a selection of representative genes validated the gene expression changes observed by the array analysis. Levels of mRNA expression of inflammation and tissue injury markers (including matrix metalloproteinases) were significantly increased in MTX-TLR2 KO mice compared to MTX-WT or healthy controls (Fig. 4C). Importantly, MTX-TLR2 KO proximal jejuna exhibited upregulation of TLR4 mRNA expression. Several drug transporters and metabolizing enzymes (ABC and CYP450) were altered in MTX-TLR2 KO (Fig. 4D), but not in MTX-WT, confirming specific defects in xenobiotic metabolism in response to chemotherapy in the context of TLR2 deficiency.

TLR2 modulates p-gp synthesis and function

Our data demonstrate that mRNA expression of *Abcb1a* was significantly decreased in the inflamed proximal jejunum of MTX-TLR2 KO mice, but not in MTX-WT (Fig. 4D). Basal mRNA expression of *Abcb1a* remained unchanged in all untreated KO models when compared to WT (Fig. 4D; data not shown). Double immunofluorescence labeling of tissue sections determined membrane expression of ABCB1/MDR1-encoded p-gp to co-localize with $CD11b^+$-staining in the lamina propria of healthy WT controls (Fig. 5A). P-gp expression was also weakly detectable at the apical pole of the intestinal epithelium (Fig. 5B). Downregulation of expression was confirmed at protein level for ABCB1/MDR1-encoded p-gp in the lamina propria of inflamed proximal jejunum of MTX-TLR2 KO mice compared to MTX-WT (Fig. 5B).

Next, we examined whether p-gp may represent a direct target of TLR2 activation in human and murine $CD11b^+$-myeloid cells. A short-term time-course analysis showed that stimulation with the synthetic TLR2 ligand PCSK of THP-1 human mononuclear cells promptly (i.e. within 5 min) yielded increased p-gp protein expression levels (Fig. 5C) followed concomitantly by a maximal 6-fold induction of *ABCB1* mRNA synthesis within 6 h of stimulation (Fig. 5D). In contrast, p-gp protein or *ABCB1* mRNA expression levels were not modulated by TLR2 stimulation with PCSK in Caco-2 cells (Fig. 5C, D), an intestinal epithelial cell line which exhibits high p-gp expression at baseline (46). Of note, we observed a decrease in *Cyp1a1* mRNA expression in the TLR2 KO proximal jejunum (Fig. 4D), as previously shown (47), but we were not able to detect any modulation of *CYP1A1* mRNA by direct TLR2 stimulation of THP-1 cells (data not shown).

Treatment with MTX induced loss of p-gp expression in THP-1 cells, which was associated with increased myeloid cell death, as evidenced by PARP (poly (ADP-ribose) polymerase) cleavage (Fig. 5E). However, prestimulation with the TLR2 ligand PCSK inhibited MTX-induced loss of p-gp expression and associated cytotoxicity. Despite MTX, prestimulation with PCSK significantly induced phosphorylation of the MKK3/6→p38 MAPK-pathway (Fig. 5E). MTX-induced loss of p-gp coincided with decreased protein expression of p38 MAPK and DUSP-1 (dual specificity phosphatase 1), which was blocked by pretreatment with the TLR2 ligand. Finally, PCSK did not modulate the level of p-gp expression in MTX-

exposed $CD11b^+$-myeloid cells from TLR2 KO mice, confirming that induction of p-gp expression requires TLR2 signaling (Fig. 5F).

To analyze p-gp function in response to TLR2 activation, we performed efflux assays to determine the ability of myeloid cells to pump out known MDR1 substrates (rhodamine 123, $DiOC_2(3)$ (38)) with or without PCSK treatment. As shown in Fig. 6A, stimulation with PCSK significantly enhanced efflux of both fluorescent labelled p-gp-transported substrates from THP-1 cells (as evidenced by a significantly higher portion of cells with decreased intracellular dye concentration). We also investigated whether TLR2 activation may directly modulate the efflux of MTX (Fig. 6B). THP-1 cells were loaded (approx. 80%) with green-fluorescent MTX for 21 hours (baseline). Subsequent stimulation with the TLR2 ligand, but not vehicle control, markedly induced extracellular transport of MTX. However, pretreatment with a specific p-gp inhibitor significantly attenuated PCSK-mediated efflux of MTX (Fig. 6C), implying p-gp-mediated transport of MTX by TLR2 signaling.

TLR2 fails to protect small intestinal tissues genetically deficient in MDR1A against DNA-damaging drug-induced apoptosis

We found that mice deficient in MDR1A developed severe acute mucosal toxicity in response to systemic MTX exposure (Fig. 7A), which was even more progressive than in mice deficient in TLR2 (Fig. 1A), and experiments had to be terminated on day 6 because of wasting disease. In contrast, control WT mice on a FVB/N background showed normal intestinal morphology after MTX treatment, similar to results for the WT mice on a C57BL/6 background (Fig. 1A). Of note, baseline levels of TLR2 mRNA expression were not altered in MDR1A deficient proximal jejunum (data not shown).

To avoid the high degree of systemic morbidity caused by *in vivo* treatment of MDR1A deficient mice with MTX, we cultured small intestinal tissues *ex vivo* from WT and MDR1A KO mice and assessed cell death in response to MTX stimulation. As shown in Fig. 7B, TUNEL assay revealed excessive DNA-damaging drug-induced apoptosis in small intestines from MDR1A KO mice in response to MTX stimulation, which persisted despite PCSK pretreatment. In contrast, small intestinal tissues from WT mice showed no increase in apoptotic cell death, confirming WT resistance to MTX-induced toxicity (Fig. 7A). Of note, cell death was slightly elevated in control small intestinal tissues from MDR1A KO mice cultured *ex vivo* when compared to control WT, which is consistent with previous findings that loss of p-gp function results in increased baseline sensitivity to stress-induced injury (48). These data confirm functional dependence between ABCB1/MDR1-encoded p-gp and TLR2 signaling in MTX-mediated intestinal mucosal damage.

Gut microbiota depletion results in increased chemotherapy-induced toxicity in WT mice, which is alleviated by TLR2 ligand supplementation

The gut microbiota contains TLR2 agonists (49). As shown in Fig. 8A-C, depletion of gut commensals by broad-spectrum antibiotics (ABx) led to increased susceptibility of WT mice to chemotherapy-induced small intestinal damage, similar to that seen in TLR2-deficient mice (Fig. 1, 2). ABx-treated WT mice exhibited severe mortality and morbidity during MTX-induced intestinal mucositis. Overall mortality rate was ~60% in ABx-treated MTX-

WT mice vs. 0% in untreated MTX-WT controls (Fig. 8A). ABx-treated MTX-WT mice showed significant inflammatory stress-induced injury of the proximal jejunum with villous atrophy, $CD11b^+$-myeloid cell infiltration and barrier dysintegrity with DNA damage, which was not evident in untreated MTX-WT controls (Fig. 8B, C). These results point to a specific association between gut commensal microbiota and protection against mucosal toxicity induced by chemotherapy treatment.

We next assessed the effect of oral supplementation with the TLR2 agonist PCSK on MTX-toxicity in gut microbiota-depleted WT mice. PCSK-supplemented ABx/MTX-WT mice demonstrated markedly decreased lethality (10%; Fig. 8A) and showed architecturally preserved proximal small intestinal mucosa without evidence of severe inflammation and DNA damage (Fig. 8B, C). These data imply that supplementation of a TLR2 ligand can rescue WT mice from exacerbated DNA damage-associated mucosal inflammation and subsequent death induced by chemotherapy after antibiotic treatment. Of note, reduced protection against chemotherapy-induced small intestinal mucositis in ABx-treated MTX-WT mice coincided with loss of p-gp expression in the lamina propria (Fig. 8C). However, supplementation with the TLR2 agonist PCSK after antibiotic therapy markedly attenuated decrease of p-gp expression by MTX in $CD11b^+$-expressing lamina propria mononuclear cells (Fig. 8C, D).

Treatment with a TLR2 ligand is effective in a preclinical model of human chemotherapy-induced mucositis

Finally, to validate that TLR2 activation also protects against chemotherapy-induced cellular DNA damage in the human small intestine, we set up a proof-of-principle experiment by culturing human duodenal pinch biopsies *ex vivo* in the presence or absence of PCSK followed by exposure to MTX in a three-dimensional Matrigel-based model. MTX alone resulted in a destructive inflammatory response (Fig. 9A), as most of the epithelial cells were lost and the lamina propria mononuclear cells within the remaining mucosal tissue showed signs of a strong DNA damage response with intense phospho-histone H2A.X staining (Fig. 9B) and loss of p-gp expression (Fig. 9C). In contrast, treatment with PCSK markedly reduced the severity of MTX-associated toxicity, as evidenced by the significantly improved biopsy pathology with a relatively high number of surviving epithelial cells (Fig. 9A) and low levels of DNA damage in the lamina propria (Fig. 9B), comparable to controls. PCSK-mediated prevention of genotoxicity was associated with inhibition of MTX-induced p-gp downregulation (Fig. 9C). These data suggest that TLR2 activation limits the toxic-inflammatory reaction and preserves assembly of the drug transporter p-gp in a preclinical model of human chemotherapy-induced intestinal mucositis.

Discussion

Intestinal mucositis is the most common complication of cancer chemotherapy. Here, we identify a previously unappreciated link between the innate immune system and chemotherapy toxicity in the gastrointestinal tract. Our results provide evidence that xenobiotic metabolism via the ABC transporter p-gp is part of the innate host defense to protect intestinal mucosal homeostasis. We show that TLR2 functions as a modulator of

ABCB1/MDR1 p-gp synthesis and activity in myeloid derived cells, driving chemotherapy drug efflux, which reduces cytotoxicity.

Our data from *in vitro* studies indicate that TLR2 activation induces sustained ABCB1/MDR1 p-gp synthesis and activity in murine and human myeloid cells. Presence of TLR2 was essential for PCSK-mediated induction of p-gp during chemotherapeutic DNA damage. ABCB1/MDR1 transcriptional activation occurs through a complex regulatory network, including the MKK3/6→p38 MAPK-pathway (50), which is shared by TLR2 signaling (51). p38 signaling has recently been implicated in cellular protection against genotoxic insults (52) and interacts with DUSP-1 in a tight balance to avoid excessive inflammatory activities in macrophages (53). Loss of DUSP-1 may increase cell susceptibility to injury (54). Future studies will need to determine whether TLR2-induced transcription factors, such as p38-mediated AP-1, may bind directly to the promoter region of the ABCB1/MDR1 gene that may distinctly drive the expression of this key ABC transporter.

Functionally, TLR2-induced p-gp mediated efflux of specific ABCB1/MDR1 substrates. The anticancer drug MTX represents one such substrate for p-gp (55). In response to TLR2 stimulation with PCSK, MTX was actively transported out of myeloid cells, reducing cellular drug accumulation and thus inhibiting drug-mediated cell death. Furthermore, our *ex vivo* and *in vivo* findings demonstrate that TLR2 activation distinctly modulates ABCB1/MDR1 p-gp function. Absence of TLR2 signaling (by either genetic deletion or depletion of the indigenous gut microbiota by antibiotics) aggravated chemotherapy-induced mucositis, which correlated with loss of p-gp in the inflamed mucosa. Remarkably, supplementation with the TLR2 ligand PCSK during chemotherapy in ABx-treated WT mice preserved p-gp expression in lamina propria mononuclear cells, which limited genotoxic stress-induced damage in the small intestine and decreased morbidity and mortality. TLR2-induced suppression of chemotoxicity in the small intestinal mucosa was essentially regulated through ABCB1/MDR1, as lack of MDR1A abolished TLR2-mediated inhibition of DNA-damaging drug-induced cytotoxicity.

ABCB1/MDR1 p-gp has been shown to transport a wide range of chemotherapy drugs. Furthermore, ABCB1/MDR1 p-gp cooperates with many xenobiotic mediators due to its overlapping substrate specificity. It is possible that TLR2 activation may broadly reduce cellular accumulation of other drugs that are p-gp substrates, such as other antineoplastics or immunosuppressive agents. Future studies will need to determine whether TLR2 signaling can be also exploited for the treatment of intestinal mucositis induced by chemotherapy drugs other than MTX. We observed significant alterations of a number of xenobiotic metabolism-associated genes in MTX-TLR2 KO proximal jejunal samples, whose products are responsible for many different steps of detoxification, including phase I and phase II drug-metabolizing enzymes and transporters. Besides ABCB1/MDR1 p-gp (55), gene expression levels of ABCC1-4 and ABCG2 were distinctly deregulated in the inflamed proximal jejunum of MTX-TLR2 KO mice. Future studies will need to test the possible impact of TLR2 signaling on these specific ATP-dependent drug transporters, which may also be involved in mediating MTX efflux (56), potentially contributing to genotoxic stress in the small intestinal mucosa.

We cannot exclude the possibility that additional cell-specific protective mechanisms of TLR2 may be involved in decreasing chemotoxicity in the small intestine - beyond modulation of the multidrug transporter ABCB1/MDR1 p-gp in $CD11b^{+}$-myeloid cells. The anti-inflammatory effects of commensal-induced TLR2 signaling in colonic epithelial cells have previously been demonstrated. TLR2 plays a key role in maintaining tight- and gap-junction-associated barrier integrity of the colonic epithelium (14, 57). Activation of TLR2 signaling may lead to repositioning of constitutive COX-2-expressing mesenchymal stem cells to the crypt, thus enhancing intestinal epithelial survival during radiation therapy (58). In addition, TLR2 controls goblet cell differentiation by selectively upregulating TFF3 expression (59). Deficient TLR2 signaling may imbalance microbiota-dependent intestinal epithelial barrier defense, facilitating mucosal injury and leading to increased susceptibility of acute and chronic colitis (14, 36). Here, we demonstrate that chemotherapy-induced mucositis in the small intestine is also associated with intestinal epithelial barrier dysfunction in TLR2 deficiency, as evidenced by disruption of cell-cell adhesion via phosphorylated ß-catenin and lack of goblet-cell specifc TFF3 in the proximal jejunum, which both may contribute to exacerbation of DNA damage–induced inflammatory and apoptotic destruction and impaired wound healing of the gastrointestinal tract (60, 61).

LPS exposure has been shown to aggravate MTX-induced intestinal mucositis in C3H/HeN, but not in TLR4-defective C3H/HeJ mice (62). Here, loss of ABCB1/MDR1 p-gp in the inflamed mucosa of MTX-TLR2 KO was associated with increased expression of TLR4. Mice deficient in MD-2 were resistant to MTX-induced damage. Deletion of MD-2 in TLR2 KO mice blocked disease exacerbation, implying that MD-2/TLR4 signaling is required for the severity of chemotherapy-induced intestinal damage in mice deficient in TLR2. We have previously demonstrated that combined loss of MDR1A and TLR2 results in increased MD-2 activation and LPS hypersensitivity, which accelerates colitis progression through ROS-mediated lysosomal damage and pyroptosis via IL-1ß (36). Others have shown that lack of signaling via Pregnane X receptor (PXR), a transcriptional regulator of ABCB1/MDR1 p-gp induction, leads to mucosal hyper-responsiveness to LPS (63). Collectively, these results imply that a distinct defect in xenobiotic defense signaling via ABCB1/MDR1 p-gp may result in compromised tolerance to LPS.

We considered that abnormal microbiota composition under chemotherapy and/or defined genetic deletion may have subverted the mucosal innate immune system towards LPS hypersensitivity. Using high-throughput 16S rRNA gene sequencing, we did not detect consistent differences in the microbiota between groups. Despite careful comparison of WT and TLR2 KO littermates, in which offspring resulted from controlled crosses of heterozygous mice, inter-individual variation of proximal jejunal samples was high, which is consistent with previous observations along the murine jejunum (64, 65). Similarly, previous work has suggested that the impact of TLR2 deficiency on the composition of the intestinal microbiota may be minimal (66). It is possible that we could have detected subtle changes or effects in considerably larger sample groups and at other time points. However, in our study, all TLR2 KO mice consistently showed the same degree of severity of genotoxic injury of the proximal jejunum in response to chemotherapy – regardless of inter-individual heterogeneity of bacterial communities, suggesting that unique microbiota changes may not represent the critical determinant of chemotherapy-induced mucosal damage.

Europe PMC Funders Author Manuscripts

Antibiotics are routinely administered to patients during anti-cancer therapy. The present study shows that antibiotic medication may have a detrimental impact on chemotherapy-elicited toxicity in the small intestine. Antibiotic pretreatment promoted chemosensitivity in WT mice that were otherwise chemotoxicity-resistant. Two recent studies suggested that microbiota depletion by antibiotics decreases the anti-tumor efficacy of chemotherapy (67, 68). Taken together, antibiotics may put patients who are being treated for cancer at increased risk of gastrointestinal toxicity and chemotherapy inefficacy. The frequent use of prophylactic antibiotics in clinical practice should therefore be re-considered. Our results suggest that specifically targeting TLR2 may offer a potential solution to prevent toxic side effects of chemotherapy in conjunction with antibiotics. Probiotic strains may constitute an alternative to reduce chemotoxicity (69), however, large-scale and randomized, placebo-controlled clinical trials are currently lacking. In a small observational study, supplementation with *Lactobacillus rhamnosus GG* showed a trend towards reducing severe diarrhea related to 5-FU-based chemotherapy in colorectal cancer patients (70), but its mechanisms of action (possibly via TLR2) were not studied.

Finally, in order to demonstrate the plausibility that TLR2 may represent a pharmacological target against chemotherapy-induced damage in the human gastrointestinal tract, we used an *ex vivo* three-dimensional model system of human duodenal biopsies cultured short term with or without PCSK and MTX. Our results show that TLR2 stimulation protected against chemotherapy-induced DNA damage, which correlated with preservation of p-gp expression. Future studies will need to assess whether single nucleotide polymorphisms within the TLR2 gene (71) may enhance individual susceptibility to chemotherapy-related gastrointestinal toxicity.

In conclusion, these studies provide the first evidence that TLR2 acts as a central regulator of xenobiotic defense via the multidrug transporter ABCB1/MDR1 p-gp. This novel mechanism may allow the innate immune system to respond to harmful xenobiotics and instruct their immediate clearance, thus efficiently protecting the host from the genotoxicity of high-dose chemotherapy and its adverse effects in the intestinal mucosa.

Supplementary Material

Refer to Web version on PubMed Central for supplementary material.

Acknowledgements

We thank Dr. Kensuke Miyake for MD-2 KO mice and Dr. Daniel K. Podolsky for anti-TFF3 antibody. We also thank the Wellcome Trust Sanger Institute's core sequencing team for carrying out the Illumina sequencing of 16S rRNA genes. This work utilized microscope equipment at the Imaging Center Essen, University Hospital of Essen (IMCES).

Grant support: This work was supported by the Deutsche Forschungsgemeinschaft (Grants CA226/8-1, CA226/9-1 and CA226/4-3 to E.C.) and intramural funding (Interne Forschungsförderung Essen (IFORES) to E.C.). Funding for P.S., J.P., A.W.W. and 16S rRNA gene sequencing was provided by The Wellcome Trust (Grant 098051); A.W.W. and The Rowett Institute of Nutrition and Health, University of Aberdeen, receive core funding support from the Scottish Government Rural and Environmental Science and Analysis Service (RESAS).

Nonstandard abbreviations used in this paper

ABx	antibiotics
dKO	double knockout
IEC	intestinal epithelial cell
KO	knockout
MDR	multidrug resistance
MPO	myeloperoxidase
MTX	methotrexate
OUT	operational taxonomic unit
PCSK	$Pam_3CysSK4$
p-gp	p-glycoprotein
PI	propidium iodide
WT	wildtype

References

1. Sonis ST, Oster G, Fuchs H, Bellm L, Bradford WZ, Edelsberg J, Hayden V, Eilers J, Epstein JB, LeVeque FG, Miller C, Peterson DE, Schubert MM, Spijkervet FKL, Horowitz M. Oral Mucositis and the Clinical and Economic Outcomes of Hematopoietic Stem-Cell Transplantation. Journal of Clinical Oncology. 2001; 19:2201–2205. [PubMed: 11304772]
2. Paci A, Veal G, Bardin C, Levêque D, Widmer N, Beijnen J, Astier A, Chatelut E. Review of Therapeutic Drug Monitoring of Anticancer Drugs Part 1 – Cytotoxics. European Journal of Cancer. 2014; 50:2010–2019. [PubMed: 24889915]
3. Keefe DM, Schubert MM, Elting LS, Sonis ST, Epstein JB, Raber-Durlacher JE, Migliorati CA, McGuire DB, Hutchins RD, Peterson DE. Updated Clinical Practice Guidelines for the Prevention and Treatment of Mucositis. Cancer. 2007; 109:820–831. [PubMed: 17236223]
4. Sonis ST. The Pathobiology of Mucositis. Nat Rev Cancer. 2004; 4:277–284. [PubMed: 15057287]
5. van Vliet MJ, Tissing WJ, Dun CA, Meessen NE, Kamps WA, de Bont ES, Harmsen HJ. Chemotherapy Treatment in Pediatric Patients with Acute Myeloid Leukemia Receiving Antimicrobial Prophylaxis Leads to a Relative Increase of Colonization with Potentially Pathogenic Bacteria in the Gut. Clin Infect Dis. 2009; 49:262–270. [PubMed: 19514856]
6. Stringer A, Al-Dasooqi N, Bowen J, Tan T, Radzuan M, Logan R, Mayo B, Keefe DK, Gibson R. Biomarkers of Chemotherapy-Induced Diarrhoea: A Clinical Study of Intestinal Microbiome Alterations, Inflammation and Circulating Matrix Metalloproteinases. Supportive Care in Cancer. 2013; 21:1843–1852. [PubMed: 23397098]
7. Haiser HJ, Turnbaugh PJ. Is It Time for a Metagenomic Basis of Therapeutics? Science. 2012; 336:1253–1255. [PubMed: 22674325]
8. Wallace BD, Wang H, Lane KT, Scott JE, Orans J, Koo JS, Venkatesh M, Jobin C, Yeh L-A, Mani S, Redinbo MR. Alleviating Cancer Drug Toxicity by Inhibiting a Bacterial Enzyme. Science. 2010; 330:831–835. [PubMed: 21051639]
9. Bjorkholm B, Bok CM, Lundin A, Rafter J, Hibberd ML, Pettersson S. Intestinal Microbiota Regulate Xenobiotic Metabolism in the Liver. PLoS One. 2009; 4:e6958. [PubMed: 19742318]
10. Cario E, Rosenberg IM, Brandwein SL, Beck PL, Reinecker HC, Podolsky DK. Lipopolysaccharide Activates Distinct Signaling Pathways in Intestinal Epithelial Cell Lines Expressing Toll-Like Receptors. J Immunol. 2000; 164:966–972. [PubMed: 10623846]

11. Cario E. Toll-Like Receptors in Inflammatory Bowel Diseases: A Decade Later. Inflamm Bowel Dis. 2010; 16:1583–1597. [PubMed: 20803699]
12. Rakoff-Nahoum S, Paglino J, Eslami-Varzaneh F, Edberg S, Medzhitov R. Recognition of Commensal Microflora by Toll-Like Receptors Is Required for Intestinal Homeostasis. Cell. 2004; 118:229–241. [PubMed: 15260992]
13. Fukata M, Michelsen KS, Eri R, Thomas LS, Hu B, Lukasek K, Nast CC, Lechago J, Xu R, Naiki Y, Soliman A, Arditi M, Abreu MT. Toll-Like Receptor-4 Is Required for Intestinal Response to Epithelial Injury and Limiting Bacterial Translocation in a Murine Model of Acute Colitis. Am J Physiol Gastrointest Liver Physiol. 2005; 288:G1055–1065. [PubMed: 15826931]
14. Cario E, Gerken G, Podolsky DK. Toll-Like Receptor 2 Controls Mucosal Inflammation by Regulating Epithelial Barrier Function. Gastroenterology. 2007; 132:1359–1374. [PubMed: 17408640]
15. Vijay-Kumar M, Aitken JD, Sanders CJ, Frias A, Sloane VM, Xu J, Neish AS, Rojas M, Gewirtz AT. Flagellin Treatment Protects against Chemicals, Bacteria, Viruses, and Radiation. J Immunol. 2008; 180:8280–8285. [PubMed: 18523294]
16. Malvin NP, Seno H, Stappenbeck TS. Colonic Epithelial Response to Injury Requires Myd88 Signaling in Myeloid Cells. Mucosal Immunol. 2012; 5:194–206. [PubMed: 22258450]
17. van Vliet MJ, Harmsen HJ, de Bont ES, Tissing WJ. The Role of Intestinal Microbiota in the Development and Severity of Chemotherapy-Induced Mucositis. PLoS Pathog. 2010; 6:e1000879. [PubMed: 20523891]
18. Thorpe DW, Stringer AM, Gibson RJ. Chemotherapy-Induced Mucositis: The Role of the Gastrointestinal Microbiome and Toll-Like Receptors. Exp Biol Med (Maywood). 2013; 238:1–6. [PubMed: 23479757]
19. Endicott JA, Ling V. The Biochemistry of P-Glycoprotein-Mediated Multidrug Resistance. Annual Review of Biochemistry. 1989; 58:137–171.
20. Schinkel AH, Smit JJ, van Tellingen O, Beijnen JH, Wagenaar E, van Deemter L, Mol CA, van der Valk MA, Robanus-Maandag EC, te Riele HP, et al. Disruption of the Mouse Mdr1a P-Glycoprotein Gene Leads to a Deficiency in the Blood-Brain Barrier and to Increased Sensitivity to Drugs. Cell. 1994; 77:491–502. [PubMed: 7910522]
21. Ho G-T, Moodie FM, Satsangi J. Multidrug Resistance 1 Gene (P-Glycoprotein 170): An Important Determinant in Gastrointestinal Disease? Gut. 2003; 52:759–766. [PubMed: 12692067]
22. Borst P, Schinkel AH. P-Glycoprotein Abcb1: A Major Player in Drug Handling by Mammals. J Clin Invest. 2013; 123:4131–4133. [PubMed: 24084745]
23. Marzolini C, Paus E, Buclin T, Kim RB. Polymorphisms in Human Mdr1 (P-Glycoprotein): Recent Advances and Clinical Relevance. Clin Pharmacol Ther. 2004; 75:13–33. [PubMed: 14749689]
24. Panwala CM, Jones JC, Viney JL. A Novel Model of Inflammatory Bowel Disease: Mice Deficient for the Multiple Drug Resistance Gene, Mdr1a, Spontaneously Develop Colitis. J Immunol. 1998; 161:5733–5744. [PubMed: 9820555]
25. Staley EM, Dimmitt RA, Schoeb TR, Tanner SM, Lorenz RG. Critical Role for P-Glycoprotein Expression in Hematopoietic Cells in the Fvb.Mdr1a(−/−) Model of Colitis. J Pediatr Gastroenterol Nutr. 2011; 53:666–673. [PubMed: 21681110]
26. Staley EM, Yarbrough VR, Schoeb TR, Daft JG, Tanner SM, Steverson D Jr. Lorenz RG. Murine P-Glycoprotein Deficiency Alters Intestinal Injury Repair and Blunts Lipopolysaccharide-Induced Radioprotection. Radiat Res. 2012; 178:207–216. [PubMed: 22780103]
27. Nones K, Knoch B, Dommels YE, Paturi G, Butts C, McNabb WC, Roy NC. Multidrug Resistance Gene Deficient (Mdr1a−/−) Mice Have an Altered Caecal Microbiota That Precedes the Onset of Intestinal Inflammation. J Appl Microbiol. 2009; 107:557–566. [PubMed: 19302324]
28. Siccardi D, Mumy KL, Wall DM, Bien JD, McCormick BA. Salmonella Enterica Serovar Typhimurium Modulates P-Glycoprotein in the Intestinal Epithelium. Am J Physiol Gastrointest Liver Physiol. 2008; 294:G1392–1400. [PubMed: 18403618]
29. Saksena S, Goyal S, Raheja G, Singh V, Akhtar M, Nazir TM, Alrefai WA, Gill RK, Dudeja PK. Upregulation of P-Glycoprotein by Probiotics in Intestinal Epithelial Cells and in the Dextran

Sulfate Sodium Model of Colitis in Mice. Am J Physiol Gastrointest Liver Physiol. 2011; 300:G1115–1123. [PubMed: 21350189]

30. Kim YK, Song YJ, Seo DW, Kang DW, Lee HY, Rhee DK, Han JW, Ahn CM, Lee S, Kim SN. Reversal of Multidrug Resistance by 4-Chloro-N-(3-((E)-3-(4-Hydroxy-3-Methoxyphenyl)Acryloyl)Phenyl)Benzamide through the Reversible Inhibition of P-Glycoprotein. Biochem Biophys Res Commun. 2007; 355:136–142. [PubMed: 17286965]
31. Wooten RM, Ma Y, Yoder RA, Brown JP, Weis JH, Zachary JF, Kirschning CJ, Weis JJ. Toll-Like Receptor 2 Is Required for Innate, but Not Acquired, Host Defense to Borrelia Burgdorferi. J Immunol. 2002; 168:348–355. [PubMed: 11751980]
32. Nagai Y, Akashi S, Nagafuku M, Ogata M, Iwakura Y, Akira S, Kitamura T, Kosugi A, Kimoto M, Miyake K. Essential Role of Md-2 in Lps Responsiveness and Tlr4 Distribution. Nat Immunol. 2002; 3:667–672. [PubMed: 12055629]
33. Salzman NH, K Hung, Haribhai D, Chu H, Karlsson-Sjoberg J, Amir E, Teggatz P, Barman M, Hayward M, Eastwood D, Stoel M, Zhou Y, Sodergren E, Weinstock GM, Bevins CL, Williams CB, Bos NA. Enteric Defensins Are Essential Regulators of Intestinal Microbial Ecology. Nat Immunol. 2010; 11:76–83. [PubMed: 19855381]
34. Tiwari RL, Singh V, Singh A, Barthwal MK. Il-1r–Associated Kinase-1 Mediates Protein Kinase Cδ-Induced Il-1β Production in Monocytes. J Immunol. 2011; 187:2632–2645. [PubMed: 21804018]
35. Cario E, Gerken G, Podolsky DK. Toll-Like Receptor 2 Enhances Zo-1-Associated Intestinal Epithelial Barrier Integrity Via Protein Kinase C. Gastroenterology. 2004; 127:224–238. [PubMed: 15236188]
36. Ey B, Eyking A, Klepak M, Salzman NH, Gothert JR, Runzi M, Schmid KW, Gerken G, Podolsky DK, Cario E. Loss of Tlr2 Worsens Spontaneous Colitis in Mdr1a Deficiency through Commensally Induced Pyroptosis. J Immunol. 2013; 190:5676–5688. [PubMed: 23636052]
37. Manichanh C, Reeder J, Gibert P, Varela E, Llopis M, Antolin M, Guigo R, Knight R, Guarner F. Reshaping the Gut Microbiome with Bacterial Transplantation and Antibiotic Intake. Genome Research. 2010; 20:1411–1419. [PubMed: 20736229]
38. Chaudhary PM, Roninson IB. Expression and Activity of P-Glycoprotein, a Multidrug Efflux Pump, in Human Hematopoietic Stem Cells. Cell. 1991; 66:85–94. [PubMed: 1712673]
39. Cario E, Golenbock DT, Visintin A, Runzi M, Gerken G, Podolsky DK. Trypsin-Sensitive Modulation of Intestinal Epithelial Md-2 as Mechanism of Lipopolysaccharide Tolerance. J Immunol. 2006; 176:4258–4266. [PubMed: 16547263]
40. Eyking A, Ey B, Runzi M, Roig AI, Reis H, Schmid KW, Gerken G, Podolsky DK, Cario E. Toll-Like Receptor 4 Variant D299g Induces Features of Neoplastic Progression in Caco-2 Intestinal Cells and Is Associated with Advanced Human Colon Cancer. Gastroenterology. 2011; 141:2154–2165. [PubMed: 21920464]
41. Schloss PD, Westcott SL, Ryabin T, Hall JR, Hartmann M, Hollister EB, Lesniewski RA, Oakley BB, Parks DH, Robinson CJ, Sahl JW, Stres B, Thallinger GG, Van Horn DJ, Weber CF. Introducing Mothur: Open-Source, Platform-Independent, Community-Supported Software for Describing and Comparing Microbial Communities. Appl Environ Microbiol. 2009; 75:7537–7541. [PubMed: 19801464]
42. Kozich JJ, Westcott SL, Baxter NT, Highlander SK, Schloss PD. Development of a Dual-Index Sequencing Strategy and Curation Pipeline for Analyzing Amplicon Sequence Data on the Miseq Illumina Sequencing Platform. Appl Environ Microbiol. 2013; 79:5112–5120. [PubMed: 23793624]
43. Quince C, Lanzen A, Davenport RJ, Turnbaugh PJ. Removing Noise from Pyrosequenced Amplicons. BMC Bioinformatics. 2011; 12:38. [PubMed: 21276213]
44. White JR, Nagarajan N, Pop M. Statistical Methods for Detecting Differentially Abundant Features in Clinical Metagenomic Samples. PLoS Comput Biol. 2009; 5:e1000352. [PubMed: 19360128]
45. Letunic I, Bork P. Interactive Tree of Life V2: Online Annotation and Display of Phylogenetic Trees Made Easy. Nucleic Acids Research. 2011; 39:W475–W478. [PubMed: 21470960]

46. Hunter J, Jepson MA, Tsuruo T, Simmons NL, Hirst BH. Functional Expression of P-Glycoprotein in Apical Membranes of Human Intestinal Caco-2 Cells. Kinetics of Vinblastine Secretion and Interaction with Modulators. J Biol Chem. 1993; 268:14991–14997. [PubMed: 8100817]
47. Do KN, Fink LN, Jensen TE, Gautier L, Parlesak A. Tlr2 Controls Intestinal Carcinogen Detoxication by Cyp1a1. PLoS One. 2012; 7:e32309. [PubMed: 22442665]
48. Smyth MJ, Krasovskis E, Sutton VR, Johnstone RW. The Drug Efflux Protein, P-Glycoprotein, Additionally Protects Drug-Resistant Tumor Cells from Multiple Forms of Caspase-Dependent Apoptosis. Proc Natl Acad Sci U S A. 1998; 95:7024–7029. [PubMed: 9618532]
49. Round JL, Lee SM, Li J, Tran G, Jabri B, Chatila TA, Mazmanian SK. The Toll-Like Receptor 2 Pathway Establishes Colonization by a Commensal of the Human Microbiota. Science. 2011; 332:974–977. [PubMed: 21512004]
50. Barančík M, Boháčová V, Kvačkajová J, Hudecová S, Krizanová O. g. Breier A. Sb203580, a Specific Inhibitor of P38-Mapk Pathway, Is a New Reversal Agent of P-Glycoprotein-Mediated Multidrug Resistance. Europ J Pharm Sci. 2001; 14:29–36.
51. Matsuzawa A, Saegusa K, Noguchi T, Sadamitsu C, Nishitoh H, Nagai S, Koyasu S, Matsumoto K, Takeda K, Ichijo H. Ros-Dependent Activation of the Traf6-Ask1-P38 Pathway Is Selectively Required for Tlr4-Mediated Innate Immunity. Nat Immunol. 2005; 6:587–592. [PubMed: 15864310]
52. Phong MS, Van Horn RD, Li S, Tucker-Kellogg G, Surana U, Ye XS. P38 Mitogen-Activated Protein Kinase Promotes Cell Survival in Response to DNA Damage but Is Not Required for the G(2) DNA Damage Checkpoint in Human Cancer Cells. Mol Cell Biol. 2010; 30:3816–3826. [PubMed: 20516219]
53. Perdiguero E, Sousa-Victor P, Ruiz-Bonilla V, Jardi M, Caelles C, Serrano AL, Munoz-Canoves P. P38/Mkp-1-Regulated Akt Coordinates Macrophage Transitions and Resolution of Inflammation During Tissue Repair. J Cell Biol. 2011; 195:307–322. [PubMed: 21987635]
54. Chi H, Barry SP, Roth RJ, Wu JJ, Jones EA, Bennett AM, Flavell RA. Dynamic Regulation of Pro- and Anti-Inflammatory Cytokines by Mapk Phosphatase 1 (Mkp-1) in Innate Immune Responses. Proc Natl Acad Sci U S A. 2006; 103:2274–2279. [PubMed: 16461893]
55. de Graaf D, Sharma RC, Mechetner EB, Schimke RT, Roninson IB. P-Glycoprotein Confers Methotrexate Resistance in 3t6 Cells with Deficient Carrier-Mediated Methotrexate Uptake. Proc Natl Acad Sci U S A. 1996; 93:1238–1242. [PubMed: 8577747]
56. Ranganathan P, McLeod HL. Methotrexate Pharmacogenetics: The First Step toward Individualized Therapy in Rheumatoid Arthritis. Arthritis & Rheumatism. 2006; 54:1366–1377. [PubMed: 16645965]
57. Ey B, Eyking A, Gerken G, Podolsky DK, Cario E. Tlr2 Mediates Gap Junctional Intercellular Communication through Connexin-43 in Intestinal Epithelial Barrier Injury. J Biol Chem. 2009; 284:22332–22343. [PubMed: 19528242]
58. Ciorba MA, Riehl TE, Rao MS, Moon C, Ee X, Nava GM, Walker MR, Marinshaw JM, Stappenbeck TS, Stenson WF. Lactobacillus Probiotic Protects Intestinal Epithelium from Radiation Injury in a Tlr-2/Cyclo-Oxygenase-2-Dependent Manner. Gut. 2012; 61:829–838. [PubMed: 22027478]
59. Podolsky DK, Gerken G, Eyking A, Cario E. Colitis-Associated Variant of Tlr2 Causes Impaired Mucosal Repair Because of Tff3 Deficiency. Gastroenterology. 2009; 137:209–220. [PubMed: 19303021]
60. Zhao J, Kim K-A, De Vera J, Palencia S, Wagle M, Abo A. R-Spondin1 Protects Mice from Chemotherapy or Radiation-Induced Oral Mucositis through the Canonical Wnt/B-Catenin Pathway. Proc Natl Acad Sci U S A. 2009; 106:2331–2336. [PubMed: 19179402]
61. Beck PL, Wong JF, Li Y, Swaminathan S, Xavier RJ, Devaney KL, Podolsky DK. Chemotherapy- and Radiotherapy-Induced Intestinal Damage Is Regulated by Intestinal Trefoil Factor. Gastroenterology. 2004; 126:796–808. [PubMed: 14988834]
62. de Koning BA, van Dieren JM, Lindenbergh-Kortleve DJ, van der Sluis M, Matsumoto T, Yamaguchi K, Einerhand AW, Samsom JN, Pieters R, Nieuwenhuis EE. Contributions of Mucosal Immune Cells to Methotrexate-Induced Mucositis. Int Immunol. 2006; 18:941–949. [PubMed: 16636014]

63. Venkatesh M, Mukherjee S, Wang H, Li H, Sun K, Benechet AP, Qiu Z, Maher L, Redinbo MR, Phillips RS, Fleet JC, Kortagere S, Mukherjee P, Fasano A, Le Ven J, Nicholson JK, Dumas ME, Khanna KM, Mani S. Symbiotic Bacterial Metabolites Regulate Gastrointestinal Barrier Function Via the Xenobiotic Sensor Pxr and Toll-Like Receptor 4. Immunity. 2014 doi:10.1016/j.immuni.2014.1006.1014.

64. Gu S, Chen D, Zhang JN, Lv X, Wang K, Duan LP, Nie Y, Wu XL. Bacterial Community Mapping of the Mouse Gastrointestinal Tract. PLoS One. 2013; 8:e74957. [PubMed: 24116019]

65. Stockinger S, Duerr CU, Fulde M, Dolowschiak T, Pott J, Yang I, Eibach D, Backhed F, Akira S, Suerbaum S, Brugman M, Hornef MW. Trif Signaling Drives Homeostatic Intestinal Epithelial Antimicrobial Peptide Expression. J Immunol. 2014; 10:1302708.

66. Ubeda C, Lipuma L, Gobourne A, Viale A, Leiner I, Equinda M, Khanin R, Pamer EG. Familial Transmission Rather Than Defective Innate Immunity Shapes the Distinct Intestinal Microbiota of Tlr-Deficient Mice. J Exp Med. 2012; 209:1445–1456. [PubMed: 22826298]

67. Iida N, Dzutsev A, Stewart CA, Smith L, Bouladoux N, Weingarten RA, Molina DA, Salcedo R, Back T, Cramer S, Dai RM, Kiu H, Cardone M, Naik S, Patri AK, Wang E, Marincola FM, Frank KM, Belkaid Y, Trinchieri G, Goldszmid RS. Commensal Bacteria Control Cancer Response to Therapy by Modulating the Tumor Microenvironment. Science. 2013; 342:967–970. [PubMed: 24264989]

68. Viaud S, Saccheri F, Mignot G, Yamazaki T, Daillere R, Hannani D, Enot DP, Pfirschke C, Engblom C, Pittet MJ, Schlitzer A, Ginhoux F, Apetoh L, Chachaty E, Woerther PL, Eberl G, Berard M, Ecobichon C, Clermont D, Bizet C, Gaboriau-Routhiau V, Cerf-Bensussan N, Opolon P, Yessaad N, Vivier E, Ryffel B, Elson CO, Dore J, Kroemer G, Lepage P, Boneca IG, Ghiringhelli F, Zitvogel L. The Intestinal Microbiota Modulates the Anticancer Immune Effects of Cyclophosphamide. Science. 2013; 342:971–976. [PubMed: 24264990]

69. Sanders ME, Guarner F, Guerrant R, Holt PR, Quigley EM, Sartor RB, Sherman PM, Mayer EA. An Update on the Use and Investigation of Probiotics in Health and Disease. Gut. 2013; 62:787–796. [PubMed: 23474420]

70. Osterlund P, Ruotsalainen T, Korpela R, Saxelin M, Ollus A, Valta P, Kouri M, Elomaa I, Joensuu H. Lactobacillus Supplementation for Diarrhoea Related to Chemotherapy of Colorectal Cancer: A Randomised Study. Br J Cancer. 2007; 97:1028–1034. [PubMed: 17895895]

71. Schröder NWJ, Schumann RR. Single Nucleotide Polymorphisms of Toll-Like Receptors and Susceptibility to Infectious Disease. The Lancet Infectious Diseases. 2005; 5:156–164. [PubMed: 15766650]

Europe PMC Funders Author Manuscripts

Europe PMC Funders Author Manuscripts

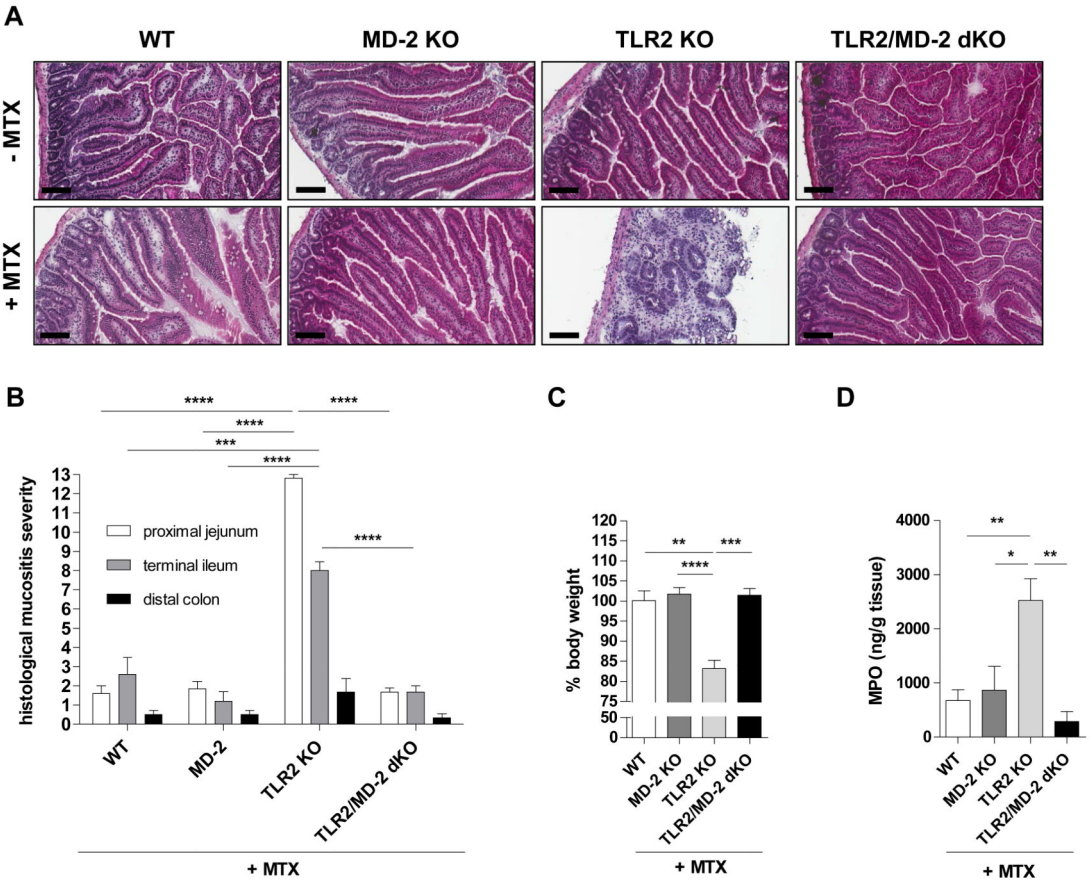

Figure 1. Genetic deletion of TLR2, but not MD-2, in mice results in severe chemotherapy-induced intestinal mucositis

Mice (WT, MD-2 KO, TLR2 KO, TLR2/MD-2 dKO) were treated with or without *i.p.* MTX [40 mg/kg BW] once daily for 4 days and sacrificed on day 7, as described in *Materials and Methods*. (A) Representative cross sections of proximal jejunum (H&E staining; scale bar, 100 μm). (B) Histological mucositis scores of proximal jejunum, terminal ileum and distal colon (n = 4-5/group). (C) Body weight change in relation to day 0 (n = 3-6/group). (D) MPO activity (n = 3-5/group). Data are presented as means ± SEM (*p < 0.05, **p < 0.01, ***p < 0.001). Pooled or representative data from at least two independent experiments are shown.

Europe PMC Funders Author Manuscripts

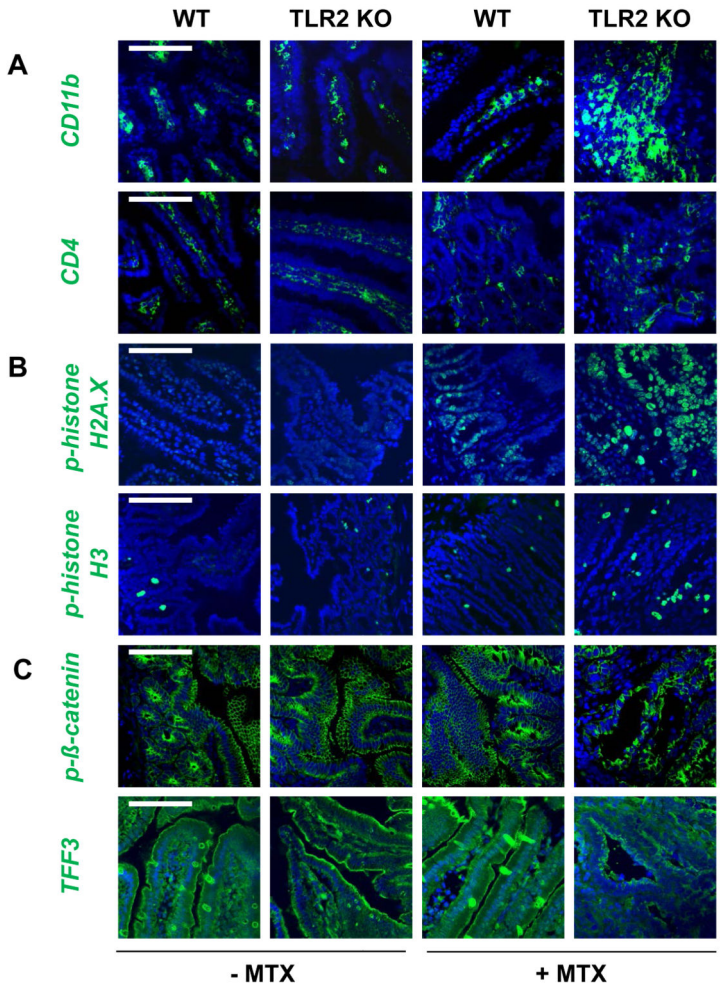

Figure 2. Chemotherapy induces inflammatory genotoxicity in the lamina propria of TLR2 KO mice

Mice (WT, TLR2 KO) were treated with or without *i.p.* MTX [40 mg/kg BW] once daily for 4 days and sacrificed on day 7, as described in *Materials and Methods*. Representative immunofluorescent staining with markers (green) for (A) inflammatory infiltration (CD11b, CD4), (B) proliferation and DNA damage (p-histone H3, p-histone H2A.X), and (C) intestinal epithelial barrier integrity (p-ß-catenin, TFF3) of proximal jejunum (n = 4/group), as assessed by optical sectioning microscopy (scale bar, 100 μm). Nuclei were counterstained with DAPI (blue). Pooled or representative data from at least two independent experiments are shown.

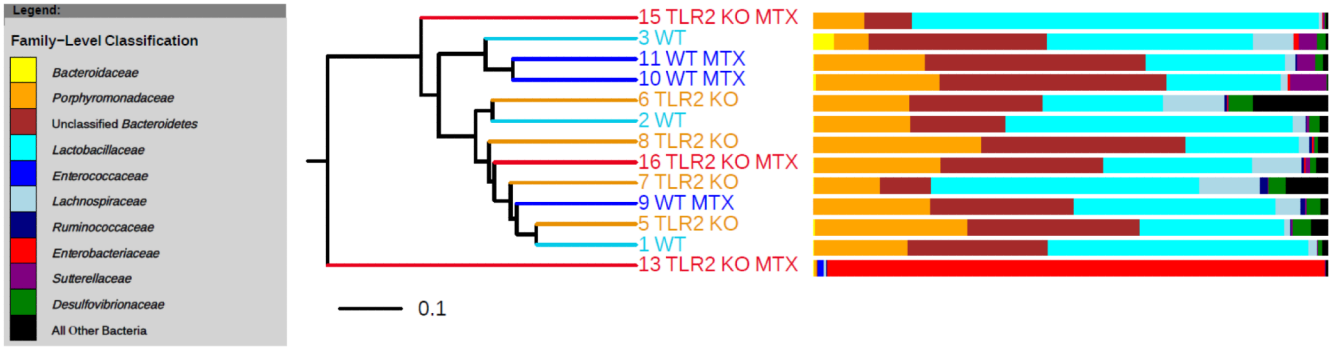

Figure 3. Dendrogram of gut microbial cluster analysis based on Bray-Curtis index

No distinct clustering patterns were deciphered when comparing overall intestinal bacterial community structure between proximal jejunal samples from the different mouse/treatment cohorts. The bacterial composition of each sample, at the Family-Level, is shown in the adjacent bar charts. Each individual mouse is numbered for reference. Mice who had received chemotherapy are indicated with “MTX”.

Europe PMC Funders Author Manuscripts

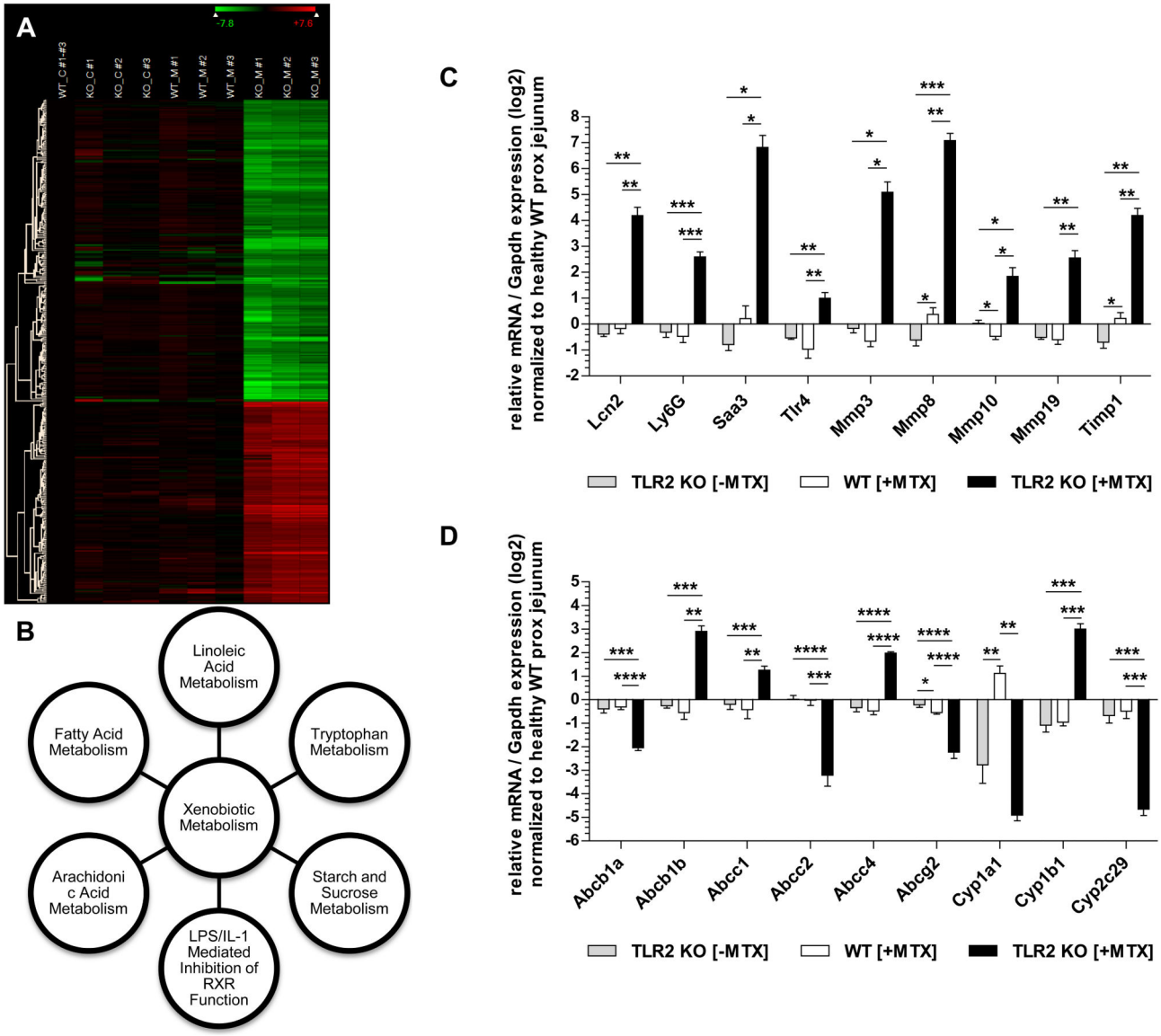

Figure 4. Gene expression analysis identifies distinct disturbances in xenobiotic metabolism of MTX-TLR2 KO proximal jejunum

(A) Hierarchical clustering analysis of selected gene regulation in proximal jejunum from WT vs. TLR2 KO mice with or without *i.p.* MTX treatment (C: control; M: MTX) on day 7, as described in *Materials and Methods*. Genes that were regulated at levels of >8-fold differential expression in comparison between the data sets “MTX-TLR2 KO” and “WT control” were included (n = 409; no duplicates). Each row corresponds to a single gene. The columns contain individual samples from 3 different mice (#1-#3), which are compared to the mean of 3 WT controls as baseline. The color scale at the top right corner of the figure uses only the range of relative expression level values from the data displayed in the heat map (log2 scale). Per-row color scaling was applied for expression levels (green, highly suppressed; black, mildly expressed; red, highly expressed). A detailed list of these selected genes is provided in Suppl. Table I. (B) Linkage of the top canonical pathways by Ingenuity

pathway analysis. A log2 ratio cutoff of 4.0 was set to focus only on genes with expression values that were most differentially regulated in the microarray data set of proximal jejunum from MTX-TLR2 KO vs. MTX-WT mice. The 140 genes identified (Suppl. Table IIIA) were linked by Ingenuity pathway analysis and statistical significance of the major canonical pathways (Suppl. Table IIIB) was determined by B-H multiple correction ($p < 0.001$). (C) + (D): Relative expression of selected genes related to (C) inflammation and tissue injury (including matrix metalloproteinases) and (D) drug transporters and metabolizing enzymes (ABC and CYP450) that were differentially regulated in proximal jejunum samples from WT vs. TLR2 KO mice (n = 5-6/group) ± MTX administration, as determined by real-time RT-PCR analysis. Results (log2 base) are shown in relation to mRNA expression for the housekeeping gene *Gapdh* and normalized to the average expression of healthy proximal jejunum from WT mice. Data are presented as means ± SEM (*$p < 0.05$, **$p < 0.01$, ***$p < 0.001$, ****$p < 0.0001$).

Europe PMC Funders Author Manuscripts

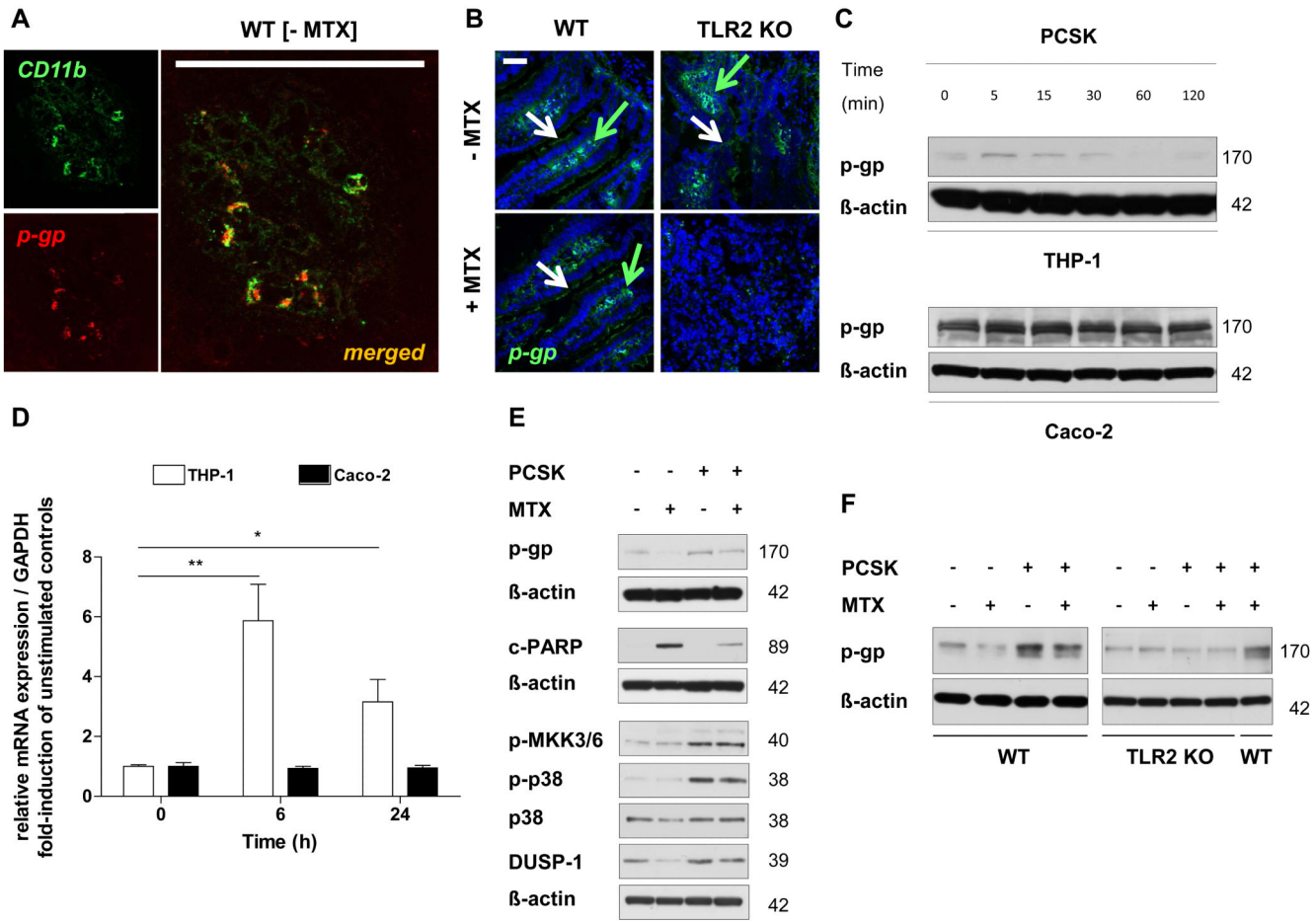

Figure 5. TLR2 activation induces synthesis of the ABC transporter ABCB1/MDR1 p-gp in human and murine CD11b$^+$-myeloid cells

(A) Representative co-localization of CD11b (green) and p-gp (red) in the lamina propria of healthy WT proximal jejunum (n = 2), as assessed by optical sectioning microscopy (scale bar, 100 μm). (B) Representative immunofluorescent staining (green) of the central efflux transporter (p-gp) in the proximal jejunum from WT and TLR2 KO mice after *i.p.* MTX administration on day 7 (n = 3/group), as assessed by optical sectioning microscopy (scale bar, 50 μm). Green arrows indicate examples of positive cells in lamina propria; white arrows indicate IEC staining. Nuclei were counterstained with DAPI (blue). (C) + (D) Time course of ABCB1/MDR1 p-gp expression in human THP-1 and Caco-2 cells after stimulation with PCSK (20 μg/ml) by (C) western blot and (D) real-time RT-PCR analysis. Results are shown in relation to mRNA expression for the housekeeping gene *GAPDH* and normalized to the average expression of unstimulated controls. Data are presented as means ± SEM (*p < 0.05, **p < 0.01). (E) Western blot analysis of p-gp expression in association with cleaved PARP and DUSP-1→p38 MAPK-pathway in human THP-1 cells after stimulation with or without PCSK (20 μg/ml) for 24 hours, washing, and incubation with MTX (10 μM) for 66 hours. (F) Western blot analysis of p-gp expression in bone marrow-derived myeloid CD11b$^+$ cells isolated from WT or TLR2 KO mice after stimulation with or

without PCSK (20 μg/ml) for 3 hours, washing and incubation with MTX (10 μM) for 21 hours. Representative results of at least two independent experiments are shown.

Europe PMC Funders Author Manuscripts

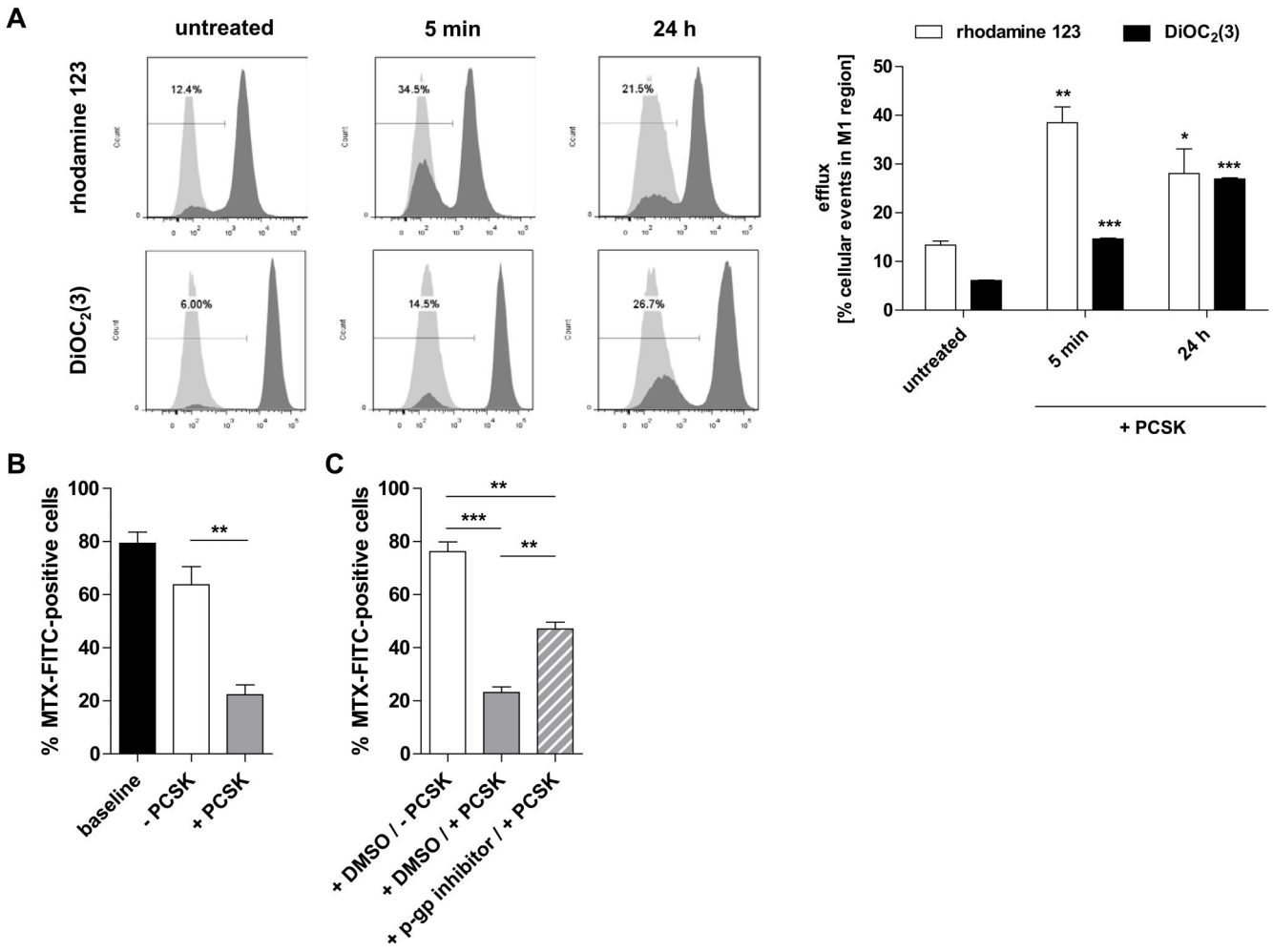

Figure 6. Functionally, stimulation of TLR2 mediates transport activity of ABCB1/MDR1 p-gp and efflux of MTX

(A) P-gp function measured by rhodamine 123 or $DiOC_2(3)$ efflux assays. THP-1 cells were left untreated for 24 hours or stimulated with PCSK (20 μg/ml) for 5 min or 24 hours, loaded with rhodamine 123 for 1 h or $DiOC_2(3)$ for 15 min on ice followed by efflux for 1 h, after which the immunofluorescence of the cell population was measured by flow cytometry. *Left panel:* efflux was quantified in terms of the fraction of cells in the M1 region of the plot (low fluorescence in light gray) as percentage of the total cells. Representative plots show the level of fluorescence versus cell counts; light grey: unloaded control cells. *Right panel:* cumulative data representing means ± SEM (n = 3 independent experiments per dye assay; *p < 0.05, **p < 0.01, ***p < 0.001: vs. untreated controls). (B) Cellular efflux of MTX in response to TLR2 stimulation. THP-1 cells were directly loaded with FL-MTX (10 μM) for 21 hours (baseline), washed and treated with or without PCSK (20 μg/ml) for 3 hours, and subjected to FACS analysis; percentages of FITC-positive cells are indicated. (C) Blockage of TLR2-mediated efflux of MTX by p-gp inhibition. THP-1 cells were pretreated with the p-gp inhibitor (10 μM) or vehicle (DMSO) for 15 min, stimulated with or without PCSK (20 μg/ml) for 5 min, washed and incubated with FL-MTX (10 μM) for 21 h. (B) + (C) Data are

presented as the means ± SEM (n = 2-3 independent experiments; **$p < 0.01$, ***$p < 0.001$).

Europe PMC Funders Author Manuscripts

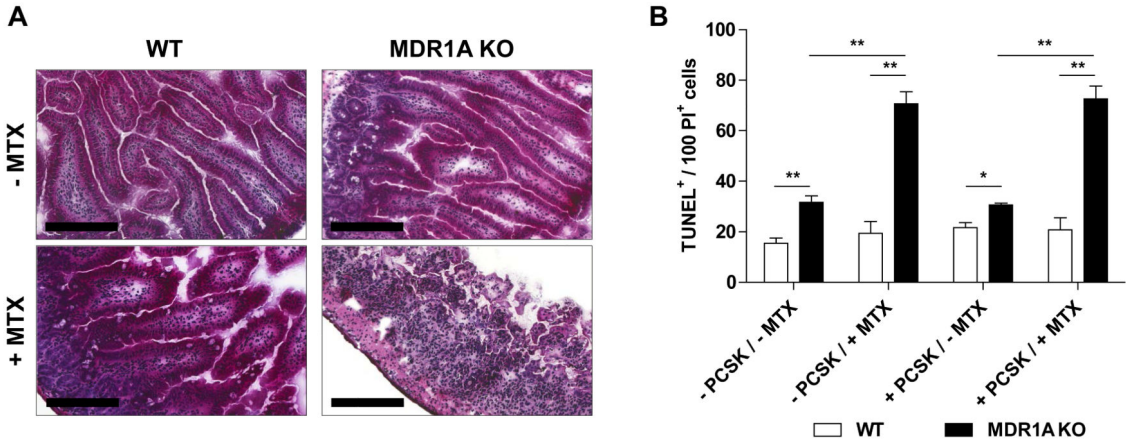

Figure 7. TLR2 ligand abolishes DNA-damaging chemotherapeutic drug-induced apoptosis in small intestinal tissues from WT but not MDR1A KO mice

(A) Mice (WT, MDR1A KO) were treated with or without *i.p.* MTX [40 mg/kg BW] once daily for 4 days and sacrificed on day 6 (n = 3-4/group), as described in *Materials and Methods*. Representative cross sections of proximal jejunum (H&E staining; scale bar, 200 μm). (B) Extent of DNA-damaging apoptosis of small intestinal tissues from WT and MDR1A KO mice cultured *ex vivo* on Matrigel monolayers after stimulation with or without the synthetic TLR2 ligand PCSK (20 μg/ml) for 30 min followed by exposure to MTX (10 μM) for 4 h, as examined by TUNEL assay. Data are presented as means ± SEM (n = 3 independent experiments; *p < 0.05, **p < 0.01).

Europe PMC Funders Author Manuscripts

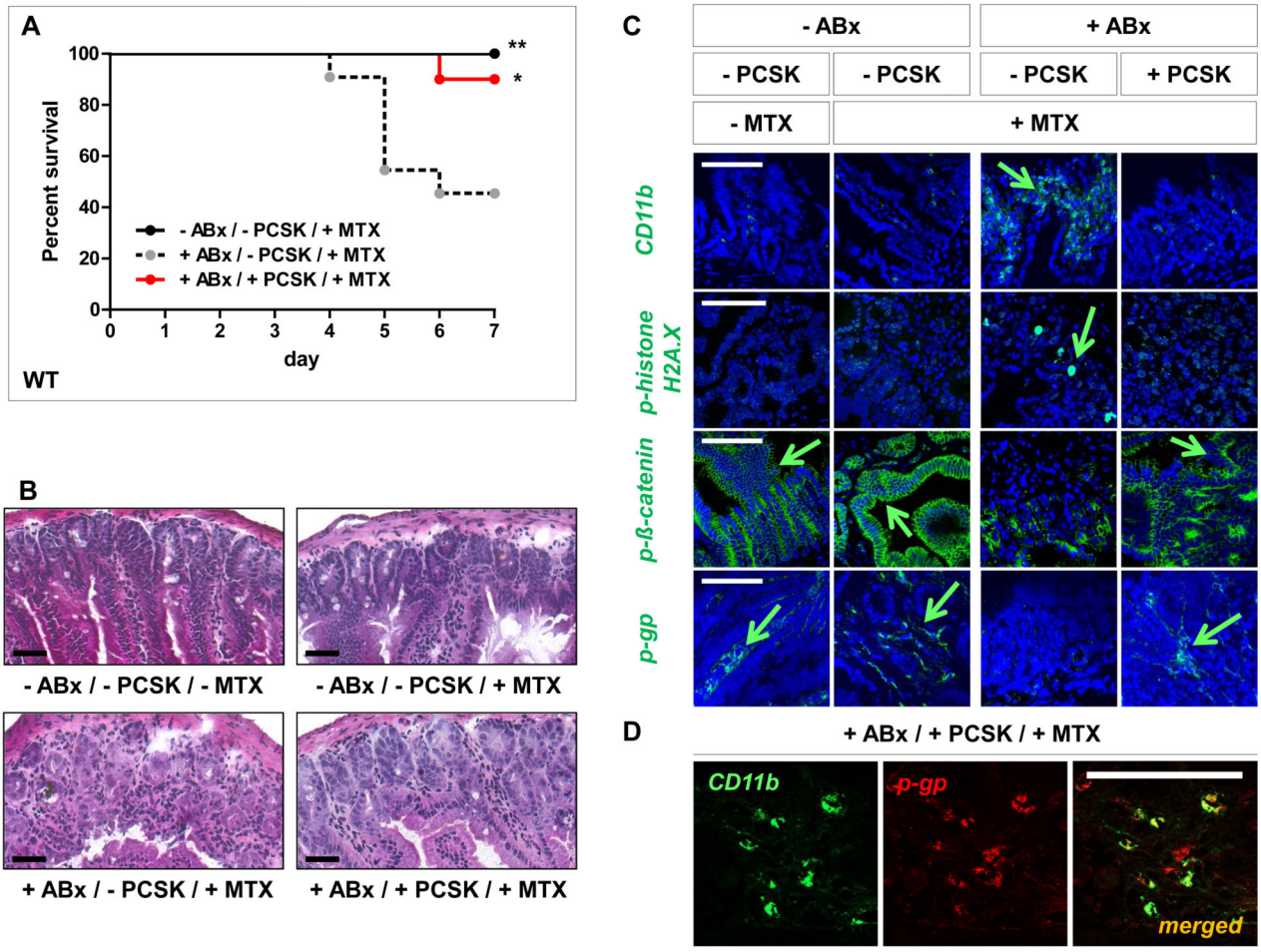

Figure 8. Gut microbiota depletion results in increased small intestinal chemotoxicity in WT mice, which is alleviated by TLR2 ligand supplementation

After gut decontamination with *p.o.* broad-spectrum antibiotics [vancomycin/imipenem; 50 mg/kg BW] for 5 days, WT mice were administered *i.p.* MTX [40 mg/kg BW] once daily for 2 days; from day −1 to maximal day 5, the mice were treated with or without *p.o.* PCSK [150 μg/ml], as described in *Materials and Methods*. Pooled data from at least two independent experiments are shown. (A) Survival analysis. Mice were monitored for survival up to day 7 post-MTX start (n = 10-12/group). Data are plotted on a Kaplan-Meier curve. *p < 0.05, **p < 0.01 (log-rank test versus "+ABx/-PCSK/+MTX"-control). (B) Representative histology of the proximal jejunum (n = 3-4/group) on day 3 (H&E; scale bar, 50 μm). (C) Representative immunofluorescent staining with markers (green) for inflammatory infiltration (CD11b), DNA damage (p-histone H2A.X), IEC barrier integrity (p-ß-catenin) and central efflux transporter (p-gp) of proximal jejunum on day 3 (n = 2/group), as assessed by optical sectioning microscopy (scale bar, 100 μm). Green arrows indicate examples of positive cells. Nuclei were counterstained with DAPI or TO-PRO-3 (blue). (D) Representative co-localization of CD11b (green) and p-gp (red) in the lamina propria of "+ABx/+PCSK/+MTX"-proximal jejunum on day 3 (n = 2/group), as assessed by optical sectioning microscopy (scale bar, 100 μm).

Europe PMC Funders Author Manuscripts

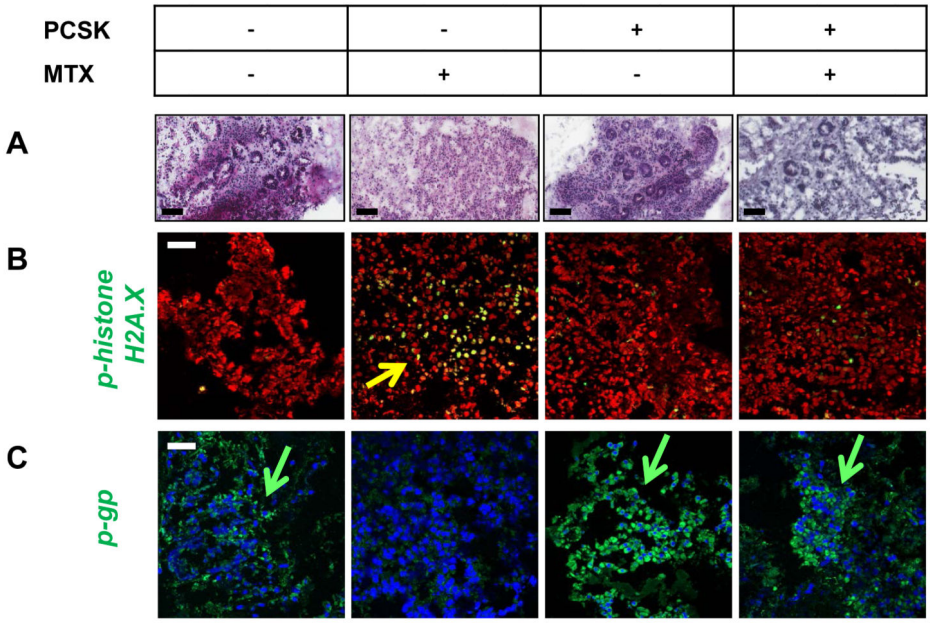

Figure 9. Treatment with the TLR2 agonist PCSK prevents chemotherapy-induced cytotoxic damage in human duodenal lamina propria mononuclear cells of patients

Human small intestine tissues were exposed to PCSK (20 μg/ml) and/or MTX (10 μM) in an *ex vivo* Matrigel-based culture model of duodenal pinch biopsies, as described in *Materials and Methods*. (A) Representative histology (H&E; scale bar, 100 μm). (B) + (C) Representative immunofluorescent staining with markers (green) for (B) DNA damage (p-histone H2A.X) and (C) central efflux transporter (p-gp), as assessed by optical sectioning microscopy. Green/yellow arrows indicate examples of positive cells in the lamina propria. Nuclei were counterstained with DAPI (red or blue). Scale bar, 50 μm.

Europe PMC Funders Author Manuscripts